

# Random cubic graph embedded in a hypercube: Entanglement spectrum and many-body localization

František Slanina<sup>1</sup>

<sup>1</sup>*Institute of Physics, Czech Academy of Sciences,  
Na Slovance 2, CZ-18200 Praha, Czech Republic\**

The schematic model of interacting spins is introduced, which combines the symmetry of hypercube with the simplicity of random regular graph with degree three, i.e. the random cubic graph. We study the localization transition in this model, which shares essential characteristics with the systems exhibiting many-body localization. Namely, we investigate the transition in terms of the entanglement entropy and entanglement spectrum. We also show that the most significant indicator of the localization transition is the failure of eigenstate thermalization hypothesis, when the distribution of matrix elements of local operators changes from Gaussian to bimodal. It also provides good estimate for the critical disorder strength.

## I. INTRODUCTION

The hypothesis that a physical system left in isolation eventually thermalizes to uniquely determined equilibrium state is the basic principle of all thermodynamics [1]. However, experimental techniques are currently available to prepare systems which violate this principle on large enough time scales to make the breakdown of thermalization physically relevant. It was observed notably in strongly interacting quantum systems well isolated from their environment. The phenomenon acquired the name many-body localization and it was reported in many experiments [2–21]. The technique used most often involves atoms trapped in an optical speckle, which forms a quasiperiodic potential, like in the Aubry-André model [22], where single-particle localization was proved. The trapped atoms can be both fermions [2, 3, 7, 9, 14] or bosons [5, 6, 14, 16, 17], the speckle can be one- as well as two-dimensional [5, 10, 15] and can be also time-periodic, thus forming a Floquet system [11]. Other experimental setups are based on nuclear spins [4, 12] ions [18] and quantum simulators and superconducting qubits [8, 13, 19–21]. Most of the experiments rely on the demonstration of persistence of initial conditions, thus manifesting non-ergodicity. From the point of view of our work the most stimulating experiments aim at measuring entanglement entropy [17, 18] which is notoriously very difficult [23].

The study of the localization phenomenon, pioneered by Anderson [24], concentrated for a long time on non-interacting systems, where the existence of localized phase was rigorously proved in various geometries, starting from the Bethe lattice [25]. However, it might be interesting to recall that already in the original Anderson's paper [24] there is a hint that localization might put in question the assumed approach to thermal equilibrium in interacting spins systems perfectly isolated from the external heat bath, which is analogous to the situation observed in recent experiments mentioned above.

Historically, the debate about the localization in many-particle interacting systems was long open, with general belief tending to the opinion that however weak interaction always destroys localization and the many-body systems can at most bear some traces of localized character that would hypothetically exist if the interaction was turned off.

Such mood changed after a series of papers [26, 27] which presented convincing arguments based on diagrammatic approaches, that weak enough interaction does not disrupt the localized character of many-body eigenstates. One of the essential ingredients was the similarity of the topology of the Fock space with a Cayley tree, at least on local level. The argument is that the localization in the many-particle Fock space then follows from the well-known localization on a Bethe lattice [25, 28].

These arguments found immediately strong support from exact diagonalization, time-dependent DMRG and numerical renormalization-group studies of specific one-dimensional Hamiltonians with on-site disorder [29–33] which was then confirmed and refined in subsequent studies [34–57]. MBL phase was then observed also in systems with random interaction, rather than random potential [58, 59], in deterministic Fibonacci chains [60], in Floquet systems [43], or in absence of disorder in gauge-invariant systems [61].

The rigorous proof of the existence of MBL state is still lacking, but current mathematical results come quite close to it. Indeed, MBL was proved in spin chains based on a very plausible (yet unproven) assumption on the eigenenergy spectrum [62, 63]. Further rigorous results concern spin systems which can be mapped on free fermions via Jordan-Wigner (JW) transform [64]. This result is sometimes erroneously considered obvious, but it is far from that due to non-locality of the JW transform. There are also rigorous results on localization in spin chains infinitesimally close to ground state [65] and on interacting systems with arbitrary (but finite in thermodynamic limit) number of particles [66, 67].

The phenomenology of MBL state is usually related to the emergence of the full set of local integrals of motion (LIOM). It is supposed that the Hamiltonian of the

\* slanina@fzu.cz

system can be written as a sum of products of these LIOMs, with coefficients which decay exponentially with distance [62, 63, 68–74]. On one side, this approach is a basis of proofs of the existence of MBL state [62, 63], on the other it serves as a starting point for investigation of the stability of MBL state with respect to small heat baths [75–77], Griffiths effects [51, 78–81] and avalanches [82–84]. However, it is not yet clear how the scheme of LIOMs works in systems with many-particle mobility edge. In fact, the very existence of MBL state with a mobility edge was questioned [85], contrary to what the exact diagonalization studies suggest [46–48, 54, 55].

The essence of the transition to MBL state is abrupt change in the character of the eigenvectors of the Hamiltonian. This manifests itself in broken ergodicity which can be measured by several witness indicators. The first witness is the level statistics, which changes from Wigner-Dyson to Poisson [29] and it was used in most of the exact diagonalization studies of MBL. The second is the entanglement entropy, where volume law is replaced by area law [86]. In ergodic phase, entanglement entropy grows linearly in the asymptotics of large sizes. For finite sizes, Page formula [87] is conjectured to hold. On top of it, exponential corrections follow from the random-matrix theory, as used in [88]. More detailed information is contained in entanglement spectrum, which has Marčenko-Pastur [89] form in the ergodic phase and qualitatively different form in MBL phase [88, 90–94]. Moreover, on the dynamic side, MBL phase is distinguished from both ergodic and single-particle Anderson localized systems by logarithmic growth of entanglement entropy (until saturation due to finite size), when started from a product state [30, 41, 42, 95].

The third witness is the breakdown of eigenvector thermalization hypothesis (ETH) [96–99]. This can be measured e. g. using the probability distribution of the matrix elements of local operators, which is expected to be Gaussian in ergodic state, but changes to bimodal form in MBL state [31, 100–102].

Together, the accumulated evidence leads to widely accepted view that MBL is a well established phase of matter. On the other hand, serious doubts do exist about observability of true MBL behavior with current approaches and available sample sizes [101, 103–105], despite efforts in developing new algorithms [106]. Further details on various aspects of MBL can be found in several recent reviews, e. g. [107–115].

In this work we come back to the early stage of the research in MBL and try to revisit a not fully investigated path. As we already mentioned, the founding arguments of the basic works [26, 27] relied on the similarity of the Fock space topology with that of a Bethe lattice, at least on a local level. In fact, local isomorphism of a graph to a tree is enough to establish exactly the transition point [28] but not enough to fully establish the nature of eigenstates. The point is that a finite Bethe lattice, or more properly a Cayley tree, is fundamentally unphysical due to the fact that the surface sites comprise finite

fraction of the total volume. This has profound implications on the character of eigenvectors [116–118]. There is a simple way out, though, namely working with (finite) random regular graphs (RRG) which are locally isomorphic to Cayley trees, but do not have any boundary by definition. The localization on RRGs was studied numerically [119–122] as well as analytically [123–126]. There is a close relation to Rosenzweig-Porter random-matrix ensembles, investigated e. g. on [127–131]. Note also the connection to the model of randomly interacting Majorana fermions [132].

Despite basic similarity, there are features of 1D MBL systems which do not have counterparts in RRG. For example, there are no global conserved quantities like total magnetization. Therefore, there is no obvious way how to define spin transport (connected to conserved magnetization) or mass transport (connected to conserved number of particles). That said, we should at the same time stress that the presence of a conserved quantity, which is needed for sensible definition of transport coefficients, is not indispensable for MBL effect itself. As an example we can mention e.g. Floquet systems [43]. The essential feature which makes RRG different is missing connection to Euclidean space in which spins or particles would reside. The same holds for spreading of entanglement, as there is no natural way how to express the Hilbert space of the system, which has the form of RRG, as a tensor product of two subsystems’ Hilbert spaces.

Therefore, to make connection between features special to MBL and those of RRG, an additional feature or invention is necessary. A successful example of this type is the Kosterlitz-Thouless (KT) scaling documented recently in certain random graphs [133]. Indeed, two-parametric KT flow was observed in phenomenological renormalization-group approaches to MBL [134–136]. These calculations rely fundamentally on 1D geometry of the system and embody the Griffiths phenomena which are believed to drive the MBL-to-ergodic transition. Neither 1D geometry nor Griffiths physics is present in random graphs studied in [133] but still KT flow is observed, which indicates that perhaps more features considered specific to MBL may be found in random graphs like RRG, if only correct path is discovered.

The main purpose of our present work is to amend the “amorphous” topology of random regular graphs so that it might provide insight to further features specific to MBL. To this end, we introduce here a class of random graphs which enable studying entanglement properties and ETH breaking. Thus, it is indispensable that the geometry of RRG contains additional structure which is isomorphic to a tensor product. To achieve that, we introduce random cubic graphs embedded into a hypercube of specified dimension. Random cubic graph is the simplest type of RRG, fixing the number of neighbors of each vertex to 3. In our case, the set of vertices coincides with the set of vertices of the hypercube and the set of edges of the cubic graph is the subset of edges of the hypercube. In order to construct such a graph, we introduce

a stochastic graph process. Although the algorithm does not sample the huge set of all allowed graphs uniformly, we believe that it produces instances which are randomized enough to provide representative information. In such a model, it is straightforward to study entanglement entropy and entanglement spectrum. We believe this model captures what is essential for the MBL transition and contains just little additional model-specific peculiarities.

## II. CONSTRUCTION OF RANDOM HAMILTONIAN

Consider a system of  $L$   $1/2$ -spins with yet unspecified interaction. The Hilbert space of such system is the set of vertices of  $L$ -dimensional hypercube

$$\mathcal{H} = \mathcal{V}_{\text{hyp}} \equiv \{|+1\rangle, |-1\rangle\}^L. \quad (1)$$

The set of edges of the hypercube consists of pairs of vertices with Hamming distance  $d_H$  exactly one

$$\mathcal{E}_{\text{hyp}} = \{\{v, v'\} : v, v' \in \mathcal{V}_{\text{hyp}} \wedge d_H(v, v') = 1\}. \quad (2)$$

We can define local spin operators acting in this space in an obvious way

$$\sigma_{i\alpha} = \mathbf{1}_1 \otimes \dots \otimes \mathbf{1}_{i-1} \otimes \sigma_\alpha \otimes \mathbf{1}_{i+1} \otimes \dots \otimes \mathbf{1}_L \quad (3)$$

where  $\sigma_\alpha$ ,  $\alpha \in \{x, y, z\}$  are the usual  $2 \times 2$  Pauli spin matrices.

We want to construct a random Hamiltonian of the system in such a way that its off-diagonal elements represent an adjacency matrix of a random graph. We want that this graph is locally similar to a random regular graph but globally reflects the hypercube geometry of the Hilbert space. Therefore, we construct a graph  $\mathcal{G} = [\mathcal{V}, \mathcal{E}]$  whose vertices coincide with the vertices of the hypercube  $\mathcal{V} = \mathcal{V}_{\text{hyp}}$  but the set of edges is only a subset of the edges of the hypercube,  $\mathcal{E} \subset \mathcal{E}_{\text{hyp}}$ . This subset is chosen randomly with the only constraint that the degree of all vertices in graph  $\mathcal{G}$  is the same, i.e. it is a special instance of a random regular graph. In this work the fixed degree will be 3, hence it is a random cubic graph. Besides the randomness in the structure of the graph, the Hamiltonian will contain also random diagonal elements. Therefore, we write the Hamiltonian as a matrix

$$H_{ij} = A_{ij}[\mathcal{G}] + \eta \xi_i \delta_{ij} \quad (4)$$

where  $A_{ij}[\mathcal{G}]$  is the adjacency matrix of the graph  $\mathcal{G}$  described above,  $\xi_i$  are i.i.d. random normally distributed numbers and the positive parameter  $\eta$  measures the strength of diagonal disorder.

It would be desirable to sample the set of graphs satisfying the above conditions with uniform probability. Due to computational difficulty in guaranteeing the uniformity, we suggest an alternative path, which is algorithmically very simple and we believe that it samples the whole

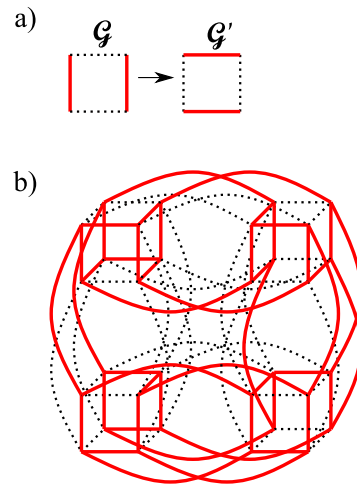


FIG. 1. In a), scheme of a single rewiring move. Full line represents an edge contained in the graph  $\mathcal{G}$  (before move) or  $\mathcal{G}'$  (after move), dotted line represents an edge contained in the hypercube, but absent in the graph. In b), an example of the cubic graph obtained by a random sequence of such moves. In this case, it is embedded in the five-dimensional hypercube ( $L = 5$ ).

set of graphs in sufficiently representative way. The algorithm proceeds in the following sequence of steps. First, choose a starting graph which is non-random, but cubic by definition. In our case, we take the first three dimensions of  $L$ -dimensional hypercube and place graph edges at all hypercube edges which go along these dimensions. This way the starting graph contains  $2^{L-3}$  disconnected cubes and is obviously cubic. Then, perform random rewiring of the graph so that in each elementary move the degrees of the touched vertices are preserved. This way, the graph is random but remains cubic all the time. Each elementary move consists in finding randomly a plaquette, i.e. a 4-cycle, on a hypercube, so that two opposite sides of the plaquette contain edges of the graph  $\mathcal{G}$  and the other two edges are empty. Then, we rewire the plaquette so that the two edges move to the empty sides of the plaquette. This way a new, changed graph  $\mathcal{G}'$  is produced. Within the plaquette, all four vertices have degree one before as well as after the move and no other vertices are influenced, so that the new graph  $\mathcal{G}'$  has the same degrees of vertices as the old graph  $\mathcal{G}$ . The move is illustrated in Fig 1a. After some time, no such plaquettes are present and the randomization algorithm stops. We also checked that the graphs produced this way are connected, i.e. they do not contain disjoint components. An example of a graph created by this algorithm is shown in Fig. 1b. In this case, it is embedded in the five-dimensional hypercube.

In order to test whether or not the rewiring algorithm described above may induce any artifacts into the results, we compared the properties of graphs obtained this way with those sampled uniformly for a small system of dimension  $L = 5$ . The results are shown in detail in the

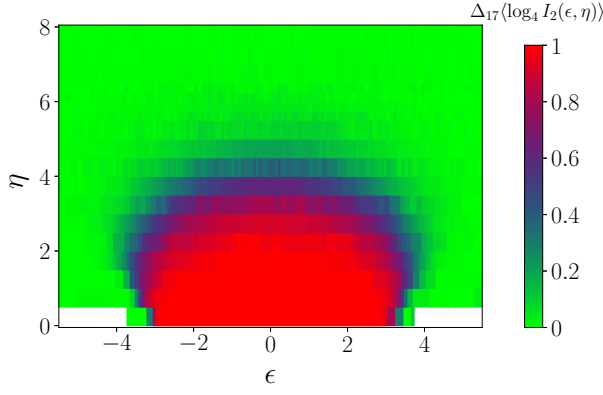


FIG. 2. Phase diagram of localization in the energy-disorder plane. Color code shows the value of the difference of log-averaged IPR between two largest system sizes used. Intermediate color (blue) provides lower estimate for the position of the mobility edge. White means absence of data.

Appendix and we can conclude that no artifacts are observed. Therefore, we shall rely on the rewiring algorithm in all what follows.

The combination of random graph and random diagonal elements constitutes the Hamiltonian (4) which represents random interaction of the  $L$  spins. Contrary to the various models based on locally interacting Heisenberg spin chains, here we have no a priori conserved quantities (like the total spin), which makes a technical advantage, because the Hilbert space does not contain disconnected segments and all vertices are statistically equivalent.

### III. SIGNATURES OF LOCALIZATION

#### A. Inverse participation ratio

We shall investigate only static features of localization. From this point of view, localization can be described as qualitative change in the dependence of various properties of eigenvectors on system size, in our case on the dimension  $L$  of the hypercube. The most direct of these properties is the inverse participation ratio (IPR), so we shall investigate it first. Let us denote  $\psi_n(\epsilon)$   $n$ -th element of the eigenvector of the Hamiltonian (4) corresponding to eigenvalue  $\epsilon$ . We define the moments

$$I_q(\epsilon) = \sum_{n=1}^{2^L} \psi_n^{2q}(\epsilon). \quad (5)$$

Beyond the obvious normalization  $I_1(\epsilon) = 1$  the lowest moment is the IPR, i.e.  $I_2(\epsilon)$ . For increasing size,  $L \rightarrow \infty$ , it should scale like

$$\ln I_2(\epsilon) \simeq \kappa_1(\epsilon)L \ln 2 + \kappa_0(\epsilon), \quad (6)$$

where  $\kappa_1(\epsilon) = 0$  in the localized phase and  $\kappa_1(\epsilon) = 1$  in the extended phase.

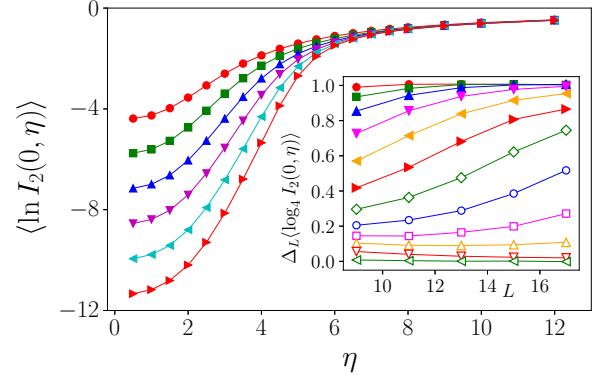


FIG. 3. Dependence of the inverse participation ratio on the disorder strength at the center of the band,  $\epsilon = 0$ . Different symbols indicate size  $L = 8$  ( $\bullet$ ), 10 ( $\blacksquare$ ), 12 ( $\blacktriangle$ ), 14 ( $\blacktriangledown$ ), 16 ( $\blacktriangleleft$ ), 18 ( $\blacktriangleright$ ). In the inset, the size dependence of the difference in log-averaged IPR. The values of disorder strength are  $\eta = 0.5$  ( $\bullet$ ), 1.5 ( $\blacksquare$ ), 2 ( $\blacktriangle$ ), 2.5 ( $\blacktriangledown$ ), 3 ( $\blacktriangleleft$ ), 3.5 ( $\blacktriangleright$ ), 4 ( $\diamond$ ), 4.5 ( $\circ$ ), 5 ( $\square$ ), 5.5 ( $\triangle$ ), 6.5 ( $\triangledown$ ), 12 ( $\triangleleft$ ).

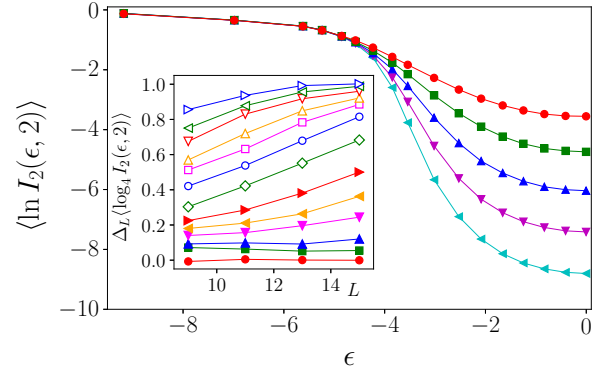


FIG. 4. Dependence of the inverse participation ratio on the energy, for disorder strength fixed at  $\eta = 2$ . Different symbols indicate size  $L = 8$  ( $\bullet$ ), 10 ( $\blacksquare$ ), 12 ( $\blacktriangle$ ), 14 ( $\blacktriangledown$ ), 16 ( $\blacktriangleleft$ ). In the inset, the size dependence of the difference in log-averaged IPR. The values of the energy are  $\epsilon = -5.620893$  ( $\bullet$ ),  $-4.232939$  ( $\blacksquare$ ),  $-4.069776$  ( $\blacktriangle$ ),  $-3.848635$  ( $\blacktriangledown$ ),  $-3.714343$  ( $\blacktriangleleft$ ),  $-3.542069$  ( $\blacktriangleright$ ),  $-3.275039$  ( $\diamond$ ),  $-3.019555$  ( $\circ$ ),  $-2.764402$  ( $\square$ ),  $-2.528745$  ( $\triangle$ ),  $-2.086117$  ( $\triangledown$ ),  $-1.658138$  ( $\triangleleft$ ),  $-0.003667$  ( $\triangleright$ ).

We investigated the properties of the eigenvectors of (4) by full numerical diagonalization of samples for even  $L$  up to size  $L = 18$ . We averaged the logarithm of IPR over many realizations of the diagonal disorder and random graph and also over all eigenvectors whose eigenvalues fall inside a narrow window  $[\epsilon - \Delta\epsilon/2, \epsilon + \Delta\epsilon/2]$ . The width of the window  $\Delta\epsilon$  was chosen empirically so that the effect of stochastic noise was minimized, while the systematic  $\epsilon$ -dependence of IPR was well visible. This way we obtained the numerical average  $\langle \ln I_2(\epsilon, \eta) \rangle$  as a function of energy  $\epsilon$ , the disorder strength  $\eta$  and system size  $L$ .

The scaling (6) holds in the asymptotic regime  $L \rightarrow \infty$ . For finite sizes we have at our disposal, we introduce the differences

$$\Delta_{\bar{L}} \langle \log_4 I_2(\epsilon, \eta) \rangle = \frac{\langle \ln I_2(\epsilon, \eta) \rangle_{L=\bar{L}-1} - \langle \ln I_2(\epsilon, \eta) \rangle_{L=\bar{L}+1}}{2 \ln 2} \quad (7)$$

and estimate the factor  $\kappa_1$  by difference between two largest values of  $L$  available i.e.  $L = 16$  and  $L = 18$

$$\kappa_1(\epsilon) \simeq \Delta_{17} \langle \log_4 I_2(\epsilon, \eta) \rangle. \quad (8)$$

In the plane energy-disorder, the quantity  $\Delta_{17} \langle \log_4 I_2(\epsilon, \eta) \rangle$  approximates the phase diagram, separating the extended and localized regime. We show this approximate phase diagram in Fig. 2. We can see that for small disorder  $\eta$  the central part of the spectrum contains extended states and the localized states are in the tails. Therefore, the system is characterized by the presence of the mobility edge. However for disorder larger than the critical value  $\eta_c$  all eigenvectors are localized.

For the purpose of establishing the value of the critical disorder the phase diagram in Fig. 2 is not sufficient, because it tells us little on the dependence on  $L$ . We show in Fig. 3 the section for the energy fixed at the center of the band,  $\epsilon = 0$ , and the size-dependence is explicitly shown. We can see that the log-averaged IPR decreases with  $L$  in the extended regime, while it remains constant in the localized regime. Even more detailed picture shows the inset in Fig. 3 where we plot the flow of the difference  $\Delta_L \langle \log_4 I_2(\epsilon, \eta) \rangle$  with increasing  $L$ . The asymptotic values 0 and 1 of this difference correspond to localized and extended phase, respectively. The flow lines go clearly to 1 for small enough  $\eta$ , but for intermediate  $\eta$  they first seem to decrease toward 0, but then turn up and tend to 1. These flow lines and their corresponding  $\eta$  should be also considered as belonging to extended phase, despite the low value of the difference  $\Delta_L \langle \log_4 I_2(\epsilon, \eta) \rangle$ . So, from this flow diagram we can guess the lower estimate for the critical disorder  $6 < \eta_c$ .

Similarly we can analyze the section of the phase diagram for fixed disorder strength. We show in Fig. 4 one such section, the dependence of log-averaged IPR on energy, for  $\eta = 2$ . For simplicity we show just one half of the dependence, for  $\epsilon < 0$ . It is sufficient due to the  $\epsilon \rightarrow -\epsilon$  symmetry of the averaged IPR. For  $\eta < \eta_c$  the spectrum contains two symmetric mobility edges at energies  $-\epsilon_m$  and  $\epsilon_m$ ; the states for  $|\epsilon| < \epsilon_m$  are extended, while the states in the tails  $|\epsilon| > \epsilon_m$  are localized. Again, we show in the inset of Fig. 4 a flow diagram, which shows how the difference in log-averaged IPR tends to 0 for localized states and to 1 for extended states. Again, for intermediate energies we can see how the flow line first seem to tend to 0, but then turns up toward 1. Therefore, the situation is similar as with the estimate of the critical disorder  $\eta_c$ . Here also, from the flow diagram we can get a lower estimate for the mobility edge, in this example for fixed  $\eta = 2$  this estimate would be  $\epsilon_m > 4.0$

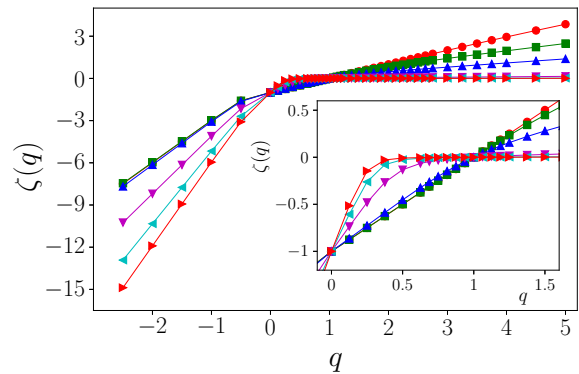


FIG. 5. Exponents for moments  $I_q$ , obtained as in Eq. (9) for  $L \leq 18$ . The eigenvectors are taken at the center of the band,  $\epsilon = 0$ . The disorder strength is  $\eta = 1$  (●), 3 (■), 4 (▲), 6 (▼), 8 (◄), 10 (►). In the inset, the detail of the same data is shown.

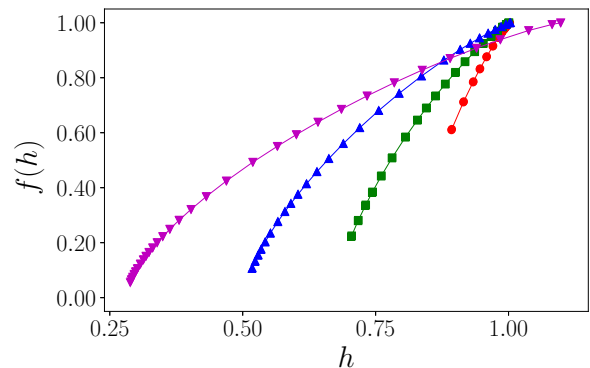


FIG. 6. Multifractal spectrum obtained by numerical inversion of the Legendre transform (10), for the data shown in Fig. 5. The disorder strength is  $\eta = 1$  (●), 2 (■), 3 (▲), 4 (▼).

## B. Multifractality

We extract the multifractal properties of the eigenvectors from the size dependence of the moments (5). As the dimension of the Hilbert space is  $N = 2^L$ , we expect for large  $L$  the asymptotic behavior

$$\langle \ln I_q \rangle \simeq -\zeta(q) L \ln 2, \quad L \rightarrow \infty. \quad (9)$$

Obviously,  $\zeta(1) = 0$  and  $\zeta(0) = -1$ . We can express the exponents  $\zeta(q)$  as Legendre transform of the multifractal spectrum  $f(h)$  [137]

$$\zeta(q) = \min_h (qh - f(h)). \quad (10)$$

In general, the function  $f(h)$  is defined on a set of non-negative numbers  $h \in \mathcal{M}$ , where  $\mathcal{M}$  can contain isolated points or continuous intervals or both. The minimum in (10) is taken over the whole definition domain  $\mathcal{M}$ . For

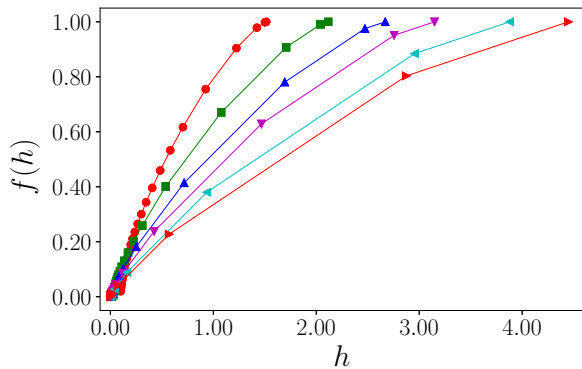


FIG. 7. Multifractal spectrum obtained by numerical inversion of the Legendre transform (10), for the data shown in Fig. 5. The disorder strength is  $\eta = 5$  (●), 6 (■), 7 (▲), 8 (▼), 10 (◀), 12 (▶).

example, homogeneous eigenvector has  $\mathcal{M} = \{1\}$  and  $f(1) = 1$ . Localized states are characterized by the presence of the point  $0 \in \mathcal{M}$ . For the eigenvectors of a matrix from GOE, one can find that  $\mathcal{M} = \{1, 3\}$ , with  $f(1) = 1$  and  $f(3) = 0$ . Non-trivial multifractal behavior occurs when the multifractal spectrum  $f(h)$  contains a continuous part [137].

We calculated the log-averaged moments for the center of the band,  $\epsilon = 0$  and extracted the exponents from the  $L$ -dependence. The result is shown in Fig. 5. From the data we can make several observations. First, for both  $q \rightarrow \infty$  and  $q \rightarrow -\infty$  the exponent  $\zeta(q)$  approaches a linear function. In fact, if  $\zeta(q)$  were a piecewise-linear function, then each linear piece would correspond to an isolated point in the set  $\mathcal{M}$ . The position of the point is given by the slope of the linear piece. This implies that genuine multifractality occurs when  $\zeta(q)$  contains a piece with continuously changing tangent. We can see in the detail shown in inset in Fig. 5 that this is the case of curves corresponding to disorder strengths  $\eta = 6, 8, 10$ . These values are therefore candidates for genuine multifractal behavior.

To see it better, we inverted numerically the Legendre transform (10) in order to find the function  $f(h)$ . We show the results in Figs. 6 and 7. Each point in these figures is a pair  $(h, f(h))$  which is compatible with the data shown in Fig. 5. In Fig. 6 we show the multifractal spectrum for weak disorder, below the expected localization threshold  $\eta_c$ . We can see that the point at  $h = 0$  is absent, i.e. states are indeed delocalized. At the same time, the function  $f(h)$  has a continuous part, extending over the interval  $[h_{\min}, 1]$ , while the lower edge  $h_{\min}$  of the multifractal spectrum is only slightly lower than 1 for very weak disorder  $\eta = 1$ , but decreases fast when the disorder strength increases. This can be interpreted as a presence of multifractal extended states. We found it impossible to decide just on the basis of available data, if it is only a finite-size effect or if it survives in the limit

$L \rightarrow \infty$ .

In Fig. 7 we show the multifractal spectrum for strong disorder, close and above the expected localization threshold  $\eta_c \gtrsim 6$ . For the disorder  $\eta = 5$  the spectrum is continuous like in the Fig. 6, but the lower edge  $h_{\min}$  is already very close to the point  $h = 0$  indicating localization. For  $\eta = 6$  and larger the point  $h = 0$  is always present and when the disorder is increasing, the numerically found points in the curve  $f(h)$  more and more accumulate around  $h = 0$ , leaving only few points at  $h > 0$ , which may ultimately be a single point at  $h = h_{\max}$ , where the value is  $f(h_{\max}) = 1$ . This suggests the following scenario in the limit  $L \rightarrow \infty$ . Exactly at the localization transition  $\eta = \eta_c$  the eigenvectors are multifractal, with  $h_{\min} = 0$ . However, in the localized phase,  $\eta > \eta_c$ , the multifractal spectrum  $f(h)$  is trivial and collapses to just two points,  $h = 0$ ,  $f(0) = 0$ , and  $h = h_{\max}$ ,  $f(h_{\max}) = 1$ .

### C. Spectral statistics

One of the widely used signatures of localization is the change in the distribution of level spacings from Poisson on localized side to Wigner-like on the extended side. The aggregate quantity which discriminates between the two is the averaged spacing ratio

$$\langle r \rangle = \left\langle \frac{\min(\epsilon_{i+1} - \epsilon_i, \epsilon_i - \epsilon_{i-1})}{\max(\epsilon_{i+1} - \epsilon_i, \epsilon_i - \epsilon_{i-1})} \right\rangle \quad (11)$$

where  $\epsilon_i$  are the eigenvalues in ascending order and the averaging is performed over the realizations of disorder and random graph and also over narrow interval of energies around the center of the band  $\epsilon = 0$ . More precisely, for given  $L$  we used  $3 \cdot 2^{L-8}$  eigenvalues closest to  $\epsilon = 0$ . We show the dependence of  $\langle r \rangle$  on disorder strength for several sizes  $L \leq 18$  in Fig. 8. For determination of the critical disorder we would like the curves cross in a single point. However, this is not the case, as observed notoriously in many numerical studies [29, 31, 46]. The crossing point shifts with increasing  $L$  to larger and larger values, thus giving no more than a lower estimate for the critical disorder, in our case  $\eta_c > 6$ . Note that this is perfectly consistent with the lower estimate deduced from the study of IPR.

## IV. ENTANGLEMENT ENTROPY

Contrary to a generic random graph, the construction used here, namely the hypercubic embedding, enables us to define in a natural way the density matrix of a subsystem of the whole system. The eigenvectors of the Hamiltonian can be indexed naturally in terms of the  $L$  binary variables  $\{s_i\}_{i=1}^L \in \{-1, 1\}^L$ . Then, for  $n = 1 + \sum_{i=1}^L 2^{i-2}(s_i + 1)$ , we have  $\psi_n(\epsilon)$  the  $n$ -th element of the eigenvector  $|\psi(\epsilon)\rangle$  corresponding to eigenvalue  $\epsilon$ . Let us

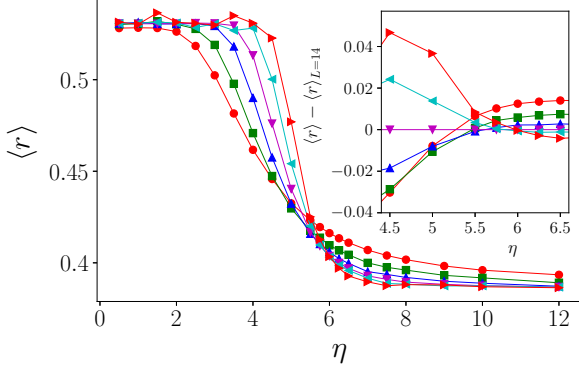


FIG. 8. Dependence of the averaged spacing ratio on the disorder strength. The system size is  $L = 8$  (●), 10 (■), 12 (▲), 14 (▼), 16 (◀), 18 (▶). In the inset, we show the detail of the area where the curves cross. For better visibility, we subtracted the data for  $L = 14$ .

now divide the system in two halves of equal size. Let the subsystem  $A$  consist of the first  $L/2$  spins, the subsystem  $B$  of the remaining ones. We define the reduced density matrix of the subsystem  $A$  only by taking trace over the degrees of freedom of the subsystem  $B$ . If we apply it on the (normalized) pure state  $|\psi(\epsilon)\rangle$  of the whole system, we have

$$\rho_{Ann'} = \sum_{n''=0}^{2^{L/2}-1} \psi_{n+2^{L/2}n''}(\epsilon) \psi_{n'+2^{L/2}n''}(\epsilon) \quad (12)$$

the matrix elements of the reduced density matrix of the subsystem  $A$ . Denote  $\lambda_n$ ,  $n = 1, \dots, 2^{L/2}$  eigenvalues of the matrix  $\rho_A$ . Then, the entanglement entropy is

$$S_e = - \sum_{n=1}^{2^{L/2}} \lambda_n \ln \lambda_n. \quad (13)$$

We omit the reference to subsystem  $A$  in the notation, as it will be always implicitly assumed throughout. Besides the aggregate quantity of entanglement entropy, we shall look also at more detailed information contained in the entanglement spectrum, more precisely the averaged density of eigenvalues

$$\mathcal{D}(\lambda) = \left\langle 2^{-L/2} \sum_{n=1}^{2^{L/2}} \delta(\lambda - \lambda_n) \right\rangle \quad (14)$$

where average is taken over realizations of the disorder and the random graph. Of course, the knowledge of entanglement spectrum gives us the average entanglement entropy

$$\langle S_e \rangle = -2^{L/2} \int \mathcal{D}(\lambda) \lambda \ln \lambda d\lambda. \quad (15)$$

For a fully random Hamiltonian, it was conjectured by Page [87] that if the system has Hilbert space of dimension  $2^L$ , then the entanglement entropy of the subsystem

which is exact half of it, is given by the following formula

$$S_P = \sum_{k=2^{L/2}+1}^{2^L} \frac{1}{k} + 2^{-1-L/2} - \frac{1}{2} \stackrel{L \rightarrow \infty}{\simeq} \frac{L}{2} \ln 2 - \frac{1}{2}. \quad (16)$$

It is commonly called the Page entropy and we shall use it as a reference value for our calculations. For the entanglement spectrum, it was shown [88, 90, 92] that for  $L \rightarrow \infty$  it approaches the Marčenko-Pastur distribution

$$2^{-L/2} \mathcal{D}(2^{-L/2} \lambda) \stackrel{L \rightarrow \infty}{\simeq} \frac{1}{2\pi} \sqrt{\frac{4-\lambda}{\lambda}}. \quad (17)$$

It can be easily checked that inserting the Marčenko-Pastur distribution (17) into the expression (15) we obtain exactly

$$\langle S_e \rangle = \frac{L}{2} \ln 2 - \frac{1}{2} \quad (18)$$

which is just the asymptotic expression for the Page entropy. Therefore, the Page entropy is the benchmark value for the entanglement entropy in the delocalized state. The fundamental feature is the volume scaling  $\langle S_e \rangle = O(L^1)$ ,  $L \rightarrow \infty$ . On the other hand, it is not as straightforward to provide similar benchmark for the localized regime. We only expect the surface scaling  $\langle S_e \rangle = O(L^0)$ ,  $L \rightarrow \infty$ . It means that entanglement entropy has a finite limit  $\lim_{L \rightarrow \infty} \langle S_e \rangle = S_{e\infty} < \infty$  and we expect that the asymptotic value as function of the disorder strength diverges at the transition, i.e.  $\lim_{\eta \rightarrow \eta_c+} 1/S_{e\infty}(\eta) = 0$ .

In Fig. 9 we show the size dependence of the difference of the entanglement entropy averaged over realizations, minus the Page entropy (16). We can see that for weak disorder this difference tends to zero, while for sufficiently large disorder it increases linearly. This distinguishes the delocalized and localized regime. However, we observe once again the same phenomenon in the dependence on  $L$ , namely that for small  $L$  the difference seems increasing, thus giving false impression of being in the localized phase, but then reaches a local maximum and eventually decreases toward zero. Therefore, this diagram can only provide a lower bound on the critical disorder strength, in this case it is even weaker than before. From Fig. 9 we can estimate that  $\eta_c > 5$ .

However, further information can be obtained from the approach to asymptotic values for  $L \rightarrow \infty$ . The approach to Page entropy in the delocalized phase is shown in Fig. 10. We found that

$$S_P - \langle S_e \rangle \simeq \Delta s + c_{\text{del}}(\eta) e^{-(\ln 2)L/2}, L \rightarrow \infty \quad (19)$$

where the constant shift  $\Delta s = 0.003$  was found empirically so that the rest is asymptotically as close to exponential as possible.

Similarly, on the localized side, we show in Fig. 11 the approach of the entanglement entropy to the asymptotic constant value

$$S_{e\infty}(\eta) - \langle S_e \rangle \simeq c_{\text{loc}}(\eta) e^{-(\ln 2)L/2}, L \rightarrow \infty. \quad (20)$$

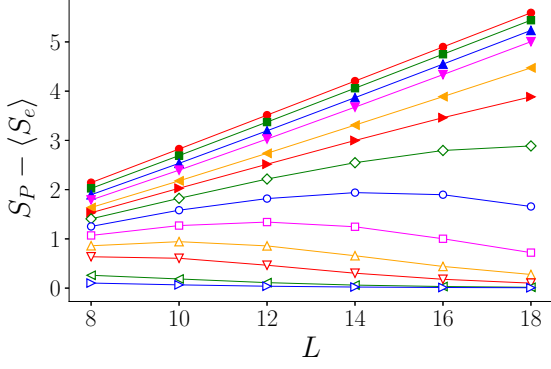


FIG. 9. Size dependence of the difference between Page entropy and entanglement entropy for disorder strengths  $\eta = 14$  ( $\bullet$ ), 10 ( $\blacksquare$ ), 8 ( $\blacktriangle$ ), 7 ( $\blacktriangledown$ ), 6 ( $\blacktriangleleft$ ), 5.5 ( $\blacktriangleright$ ), 5 ( $\diamond$ ), 4.5 ( $\circ$ ), 4 ( $\square$ ), 3.5 ( $\triangle$ ), 3 ( $\nabla$ ), 2 ( $\triangleleft$ ), 1 ( $\triangleright$ ).

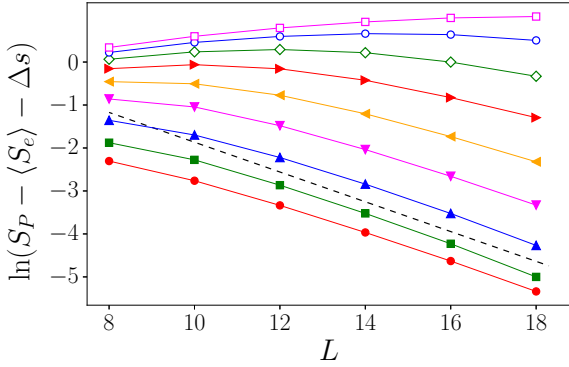


FIG. 10. Exponential approach to the Page entropy with increasing system size, in the delocalized phase. The disorder strengths are  $\eta = 1$  ( $\bullet$ ), 1.5 ( $\blacksquare$ ), 2 ( $\blacktriangle$ ), 2.5 ( $\blacktriangledown$ ), 3 ( $\blacktriangleleft$ ), 3.5 ( $\blacktriangleright$ ), 4 ( $\diamond$ ), 4.5 ( $\circ$ ), 5 ( $\square$ ). The dashed line is the dependence  $S_P - S_e - \Delta s \propto e^{-(\ln 2)L/2}$ .

The asymptotic constants  $S_{e\infty}(\eta)$  provide an information about the localization transition. As shown in the inset of Fig. 11, the inverse  $1/S_{e\infty}(\eta)$  approaches linearly zero at value  $\eta_c = 5.6(1)$ . We can see that this estimate gives a value which is slightly below the lower estimate obtained e.g. from the study of IPR. The explanation might be that the approach of  $1/S_{e\infty}(\eta)$  is actually sub-linear, rather than linear in the vicinity of the transition.

We expect that the coefficients  $c_{\text{del}}(\eta)$  and  $c_{\text{loc}}(\eta)$  of the finite-size corrections diverge when we approach to the transition. We show in Fig 12 their dependence on the disordered strength. Indeed, we can see that both of these coefficients increase in expected sense. On this basis, we can deduce weak bounds on the critical disorder  $5 < \eta_c < 7.5$ , but the assumed divergence is not clear enough to provide better quantitative estimate of the value of the critical disorder.

Interestingly, the approach follows the same exponen-

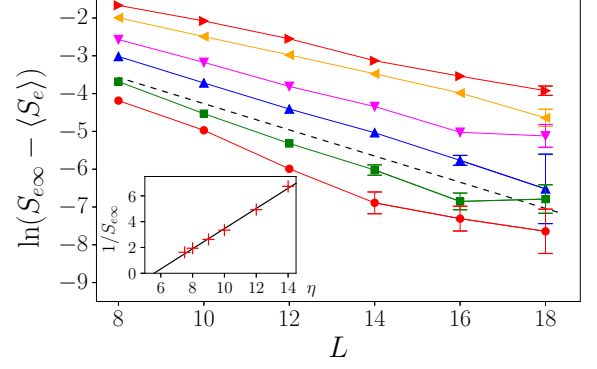


FIG. 11. Exponential approach of the entanglement entropy to the asymptotic constant  $S_{e\infty}$  with increasing system size, in the localized phase. The disorder strengths are  $\eta = 14$  ( $\bullet$ ), 12 ( $\blacksquare$ ), 10 ( $\blacktriangle$ ), 9 ( $\blacktriangledown$ ), 8 ( $\blacktriangleleft$ ), 7.5 ( $\blacktriangleright$ ). Where not shown, the error bars are smaller than the symbol size. The dashed line is the dependence  $S_{e\infty} - S_e \propto e^{-(\ln 2)L/2}$ . In the inset, the dependence of the inverse of the asymptotic value of the entanglement entropy on disorder strength. The straight line fits the data and serves to estimate the critical point  $\eta_c$  of the localization transition.

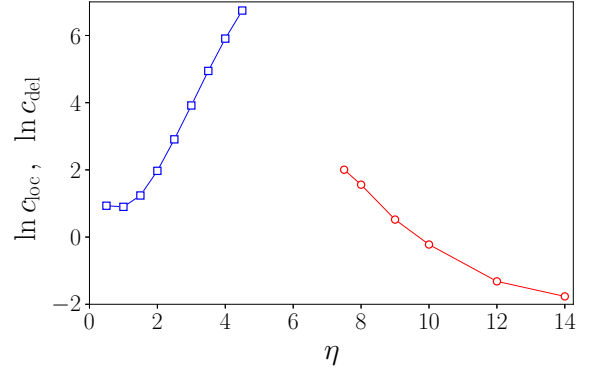


FIG. 12. Dependence of the coefficients in the finite-size corrections (19) and (20) on the disorder strength. The symbols distinguish  $c_{\text{del}}$  ( $\square$ ) and  $c_{\text{loc}}$  ( $\circ$ ).

tial law as in the delocalized phase. In fact, when we realize that  $N_A = 2^{L/2}$  is the dimension of the Hilbert space of the subsystem  $A$ , we recognize in both the exponential laws in (19) and (20) the leading  $1/N_A$  correction.

More detailed information is contained in the entanglement spectrum (14). It was already noted that the spectrum qualitatively changes its character when we go from the delocalized to localized phase [88, 90–94]. In the work [88] the authors studied the changes in the shape of the entanglement spectrum when the transition is approached from the delocalized phase and used it to calculate the correlation length. We shall use the methodology of [88] to see the qualitative change. In delocalized phase, the spectrum  $\mathcal{D}(\lambda)$  approaches the Marčenko-Pastur shape in the thermodynamic limit. It is charac-

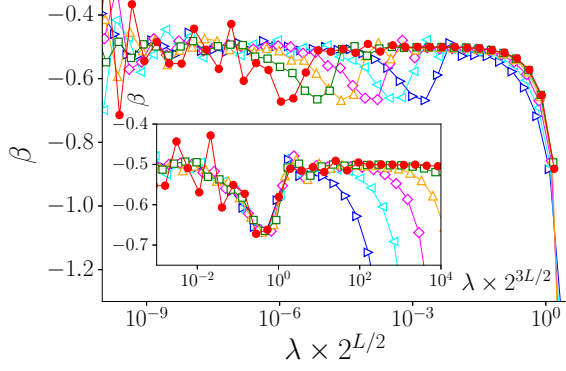


FIG. 13. Logarithmic derivative of the entanglement spectrum, for  $\eta = 1$ . In the inset, the same data scaled differently. The symbols correspond to the sizes  $L = 8$  ( $\triangleright$ ),  $10$  ( $\triangleleft$ ),  $12$  ( $\diamond$ ),  $14$  ( $\triangle$ ),  $16$  ( $\square$ ),  $18$  ( $\bullet$ ).

terized by  $\lambda^{-1/2}$  singularity for  $\lambda \rightarrow 0$ . The value of the exponent is better extracted using the logarithmic derivative

$$\beta(\lambda) = \frac{\lambda}{\mathcal{D}} \frac{d\mathcal{D}(\lambda)}{d\lambda}. \quad (21)$$

In delocalized phase, and for large  $L$ , the spectrum is supposed to be close to Marčenko-Pastur, which has

$$\beta_{MP}(\lambda) = -\frac{2}{4 - \lambda 2^{L/2}} \quad (22)$$

and indeed the exponent is  $\beta(\lambda) \rightarrow -1/2$  for  $\lambda \rightarrow 0$ .

We show in Fig. 13 the numerically obtained function  $\beta(\lambda)$  for weak disorder  $\eta = 1$  which is supposed to be deep in the delocalized phase. The formula (22) suggests the scaling  $\lambda \sim 2^{-L/2}$  of the characteristic eigenvalues, therefore we plot  $\beta$  as function of  $\lambda 2^{L/2}$  for different sizes  $L$ . We can see that indeed, with such rescaling of  $\lambda$  the spectrum approaches very well to the Marčenko-Pastur formula. However, we notice also a systematic contribution which vanishes in thermodynamic limit when plotted in scaling  $\lambda 2^{L/2}$ , but remains stable, when the function  $\beta$  is plotted against the variable  $\lambda 2^{3L/2}$ . It implies that besides the universal characteristic scale  $\lambda \sim 2^{-L/2}$  there is also another, model-dependent characteristic scale  $\lambda \sim 2^{-3L/2}$ . This should reveal itself in the next-to-leading finite-size corrections to the entanglement entropy. However, this is out of reach of the current numerical results. Note that similar feature observed in Ref. [88] had consequences already in the leading finite-size corrections.

We found that this characteristic energy scale reflects the approach to the localization transition. Indeed, we denote  $E = \lambda_{\min} 2^{3L/2}$  the position of the minimum of  $\beta$  seen in inset of Fig. 13. Then, the value of  $-\log_{10} E$  seems to diverge when we approach the critical disorder, as shown in Fig. 14. In the localized phase the minimum disappears completely. This suggests that there is a

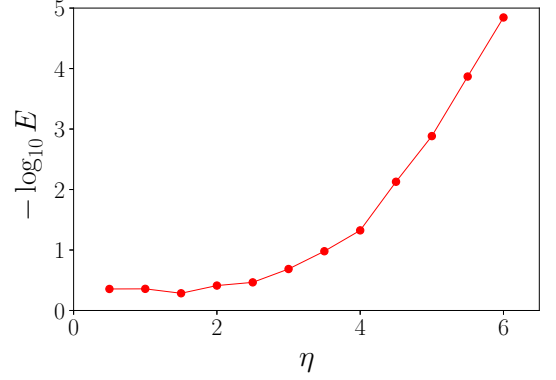


FIG. 14. Logarithm of the position of the minimum of  $\beta$  in the entanglement spectrum, depending on the disorder strength. For values  $\eta > 6$  there are no data, because the minimum disappears in localized phase.

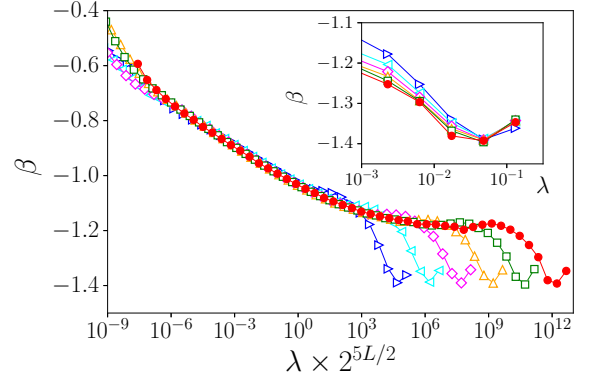


FIG. 15. Logarithmic derivative of the entanglement spectrum, for  $\eta = 12$ . In the inset, the same data scaled differently. The symbols correspond to the sizes  $L = 8$  ( $\triangleright$ ),  $10$  ( $\triangleleft$ ),  $12$  ( $\diamond$ ),  $14$  ( $\triangle$ ),  $16$  ( $\square$ ),  $18$  ( $\bullet$ ).

typical time scale  $1/E$  that goes to infinity at localization threshold.

In the localized phase, the spectrum looks completely different. We show in Fig. 15 the numerically obtained function  $\beta(\lambda)$  for strong disorder  $\eta = 12$  which is supposed to be deep in the localized phase. In absence of a clear guiding principle as to the characteristic scaling of the eigenvalues, we proceeded empirically and found that the best data collapse is achieved when  $\beta$  is plotted against  $\lambda 2^{5L/2}$ . The data collapse stretches over many decades. However, at the upper edge of the spectrum we found that  $\beta$  is simply a function of  $\lambda$ , as shown in the inset of Fig. 15. Having in mind that it is the upper edge of the spectrum that dominates the entanglement entropy (15), the observed scaling  $\lambda \sim (2^{-L/2})^0$  at the upper edge is consistent with surface scaling  $\langle S_e \rangle = O(1)$  for  $L \rightarrow \infty$ .

## V. EIGENSTATE THERMALIZATION HYPOTHESIS

Localization can be viewed either as suppression of transport or as broken ergodicity or as lack of thermalization. The latter approach is formalized in terms of violation of the Eigenstate thermalization hypothesis (ETH) [96–99]. Stated in rather simplified formulation, ETH assumes that matrix elements of local observables  $\mathcal{O}$  in any narrow interval in highly excited part of the spectrum behave in the following generic way

$$\langle \psi_n | \mathcal{O} | \psi_m \rangle = g(\epsilon_n) \delta_{nm} + \xi_{mn} h\left(\frac{1}{2}(\epsilon_n + \epsilon_m), \epsilon_n - \epsilon_m\right) \quad (23)$$

where  $\xi_{mn}$  are normally distributed random variables and  $g(\epsilon)$  and  $h(\epsilon, \omega)$  are smooth functions of their arguments. It is an analog and generalization of the spectral hypothesis stating that a portion of the spectrum in highly excited states behaves like a spectrum of a random matrix and it depends only on the symmetry of the system, whether it belongs to orthogonal, unitary or symplectic ensemble, while the details of the Hamiltonian are irrelevant. In the case of ETH, the basic notion behind is the equivalence of statistical ensembles. In addition to canonical and microcanonical ensembles, we consider also eigenstate ensemble, which is nothing else than a pure state of the system. If we consider a local observable, we can think of a part of the system containing the support of that observable as a small but still macroscopic subsystem. If the equivalence of ensembles holds for the whole system, specifically if microcanonical and eigenstate ensembles were equivalent, the average of the local observable would be the same in both cases, with Gaussian fluctuations on top of it. This is in words what (23) expresses as formula.

ETH may fail in a number of ways. The most obvious is that the functions  $g(\epsilon)$  and  $h(\epsilon, \omega)$  are not smooth, but instead fluctuate wildly, giving in fact very different values for each eigenstate. Another way of breaking ETH is having broad or long-tailed distribution of the random variables  $\xi_{mn}$ , instead of a Gaussian one. To see if ETH is broken or not we investigated the histograms of the diagonal and off-diagonal elements of the spin operators, defined in (3). Let us denote the matrix element of the  $z$ -component of the spin operator at site  $i$  as  $\sigma_{iznm} = \langle \psi_n | \sigma_{iz} | \psi_m \rangle$ . We take the eigenvectors corresponding to energies within a narrow interval  $I_\Delta = [-\Delta, \Delta]$  around the center of the band. Actually the interval was fixed so that it contained  $N_\Delta = 3 \cdot 2^{L-8}$  eigenvalues closest to zero. This distribution is subsequently averaged over site  $i = 1, \dots, L$ , and finally also over realizations of the disorder. So, we define

$$P_{\text{diag}}(\sigma) = \left\langle \frac{1}{L} \sum_{i=1}^L \frac{1}{N_\Delta} \sum_{\substack{n \\ \epsilon_n \in I_\Delta}} \delta(\sigma - \sigma_{iznn}) \right\rangle \quad (24)$$

for the diagonal elements and similarly

$$P_{\text{off}}(\sigma) = \left\langle \frac{1}{L} \sum_{i=1}^L \frac{1}{N_\Delta - 1} \sum_{\substack{n \\ \epsilon_n \in I_\Delta \\ \epsilon_{n+1} \in I_\Delta}} \delta(\sigma - \sigma_{iznn+1}) \right\rangle \quad (25)$$

for the off-diagonal matrix elements between adjacent energy levels. Of course, both of these distributions are defined on the interval  $-1 \leq \sigma \leq 1$ .

We show in Fig. 16 histograms of the diagonal elements from the largest size studied,  $L = 18$  and for various disorder strengths. We can clearly see that the distribution is centered at zero and close to Gaussian for weak disorder. Close to the transition the distribution widens and starts to cover the whole allowed interval  $\sigma \in [-1, 1]$ . In the localized phase, the distribution totally changes character and becomes bimodal, peaked around the two edge values  $\sigma = -1$  and  $\sigma = 1$ . This is a clear sign of violation of ETH. Note that similar behavior was already observed in earlier works [31, 100–102]. We looked also on the off-diagonal elements. In Fig. 17 we show the histogram for weak disorder,  $\eta = 1$ , and three system sizes. We can see that the distribution is close to Gaussian and moreover, its width decreases with increasing size. The same size dependence was observed also in the distribution of diagonal elements at weak disorder (not shown). This indicates, that ETH as formulated by the ansatz (23) is satisfied in the delocalized phase and the variance of the random variables  $\xi_{nm}$  decreases in the thermodynamic limit. In the localized phase, the off-diagonal elements behave differently from the diagonal ones. In Fig. 18 we show the histogram for  $\eta = 12$  and three different sizes. We can see, that the distribution is again centered at zero as in the delocalized phase, but the shape of the distribution is no more Gaussian, but close to a power law  $P_{\text{off}}(\sigma) \propto |\sigma|^{-\gamma}$ . For the data in Fig. 18 we estimated the exponent about  $\gamma \simeq 1.2$ . However, this value seems to depend on the disorder strength  $\eta$ , so it cannot be considered a universal exponent.

The above observations suggest the following scenario of the violation of the ETH as stated in (23), when we go from the delocalized into the localized phase. First, in the limit  $L \rightarrow \infty$ , the function  $g(\epsilon)$  is asymptotically close to 0 for all energies in the delocalized phase. On the other hand  $g(\epsilon) \in \{-1, 1\}$  in the localized phase and which of the two values holds for a given energy level  $\epsilon_n$  is essentially a random choice with equal probability. Moreover, the random variables  $\xi_{nm}$  are normally distributed, as assumed in ETH, in the delocalized phase, but become heavy-tailed, probably power-law distributed, in the localized phase.

The distributions  $P_{\text{diag}}(\sigma)$  and  $P_{\text{off}}(\sigma)$  are very instructive, but mix together the level-to-level variability in matrix element (which is of main concern here) with site-to-site and even worse, with sample-to-sample variability. These variations are better separated in the aggregate

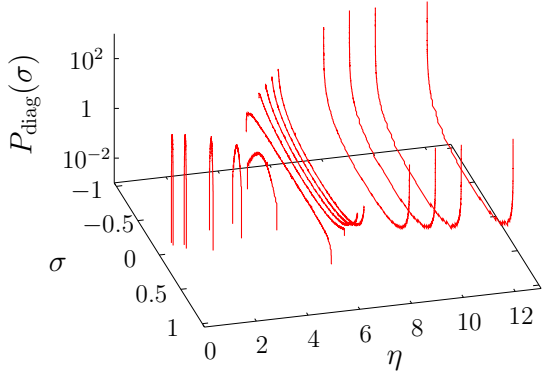


FIG. 16. Distribution of the values of the diagonal elements of the local spin operators, for several disorder strengths  $\eta$ .

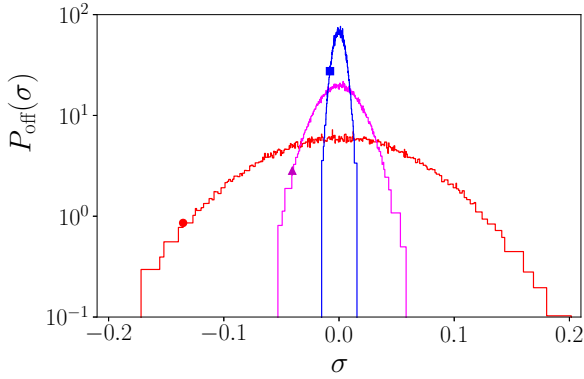


FIG. 17. Distribution of the values of the off-diagonal elements of the local spin operators, for disorder strength  $\eta = 1$ . Different curves belong to different system sizes, according to the attached symbols,  $L = 10$  (●),  $14$  (▲), and  $18$  (■).

quantity

$$R = \left\langle \frac{1}{L} \sum_{i=1}^L \left( \frac{1}{N_{\Delta}} \sum_{\substack{n \\ \epsilon_n \in I_{\Delta}}} \sigma_{iznn}^2 - \left( \frac{1}{N_{\Delta}} \sum_{\substack{n \\ \epsilon_n \in I_{\Delta}}} \sigma_{iznn} \right)^2 \right) \right\rangle \quad (26)$$

which first calculates variance of level-to-level fluctuations and then makes site and disorder average. We show in Fig. 19 how it depends on the disorder strength. In the delocalized phase the level-to-level fluctuations are low, as the ETH predicts smooth dependence on energy in function  $g(\epsilon)$ , which for narrow energy interval which we use means effectively independence on energy level. The remaining variance is due to superimposed Gaussian fluctuations, but we have already seen, that their variance diminishes when  $L \rightarrow \infty$ . So, we expect low, asymptotically zero, value of  $R$  in the delocalized phase. This is indeed observed in Fig. 19. On the contrary, in the localized phase, the values are either  $+1$  or  $-1$  randomly

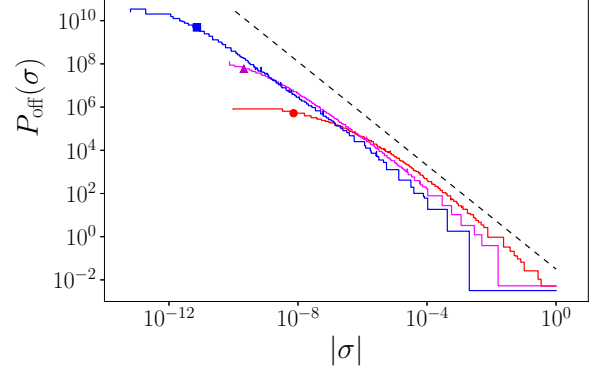


FIG. 18. Distribution of the values of the off-diagonal elements of the local spin operators, for disorder strength  $\eta = 12$ . Different curves belong to different system sizes, according to the attached symbols,  $L = 10$  (●),  $14$  (▲), and  $18$  (■). The dashed line is the power  $\propto |\sigma|^{-1.2}$ .

scattered among the levels, so that the level-to-level fluctuations are close to 1. Hence, in thermodynamic limit we expect  $R(\eta) = 1$  for  $\eta > \eta_c$  and  $R(\eta) = 0$  for  $\eta < \eta_c$ . The data shown in Fig. 19 support this expectation. The picture resembles that of the level spacings shown in Fig. 8, but we believe that  $R$  is principally better signature of the localization transition than the spacing ratio  $\langle r \rangle$ . First,  $R$  is in principle directly measurable quantity, limited only by the experimental accessibility of creating pure states. From the side of numerical simulations, as is the case of this work,  $R$  is also a much better measure. The curves of  $R(\eta)$  for increasing size  $L$  do not cross in exactly the same point, but the shift of the crossing point is substantially weaker than it is in the case of  $\langle r \rangle$ , as can be seen in comparison of insets in Figs 8 and 19. On the basis of Fig. 19 we estimate the critical disorder strength as  $\eta_c = 6.1 \pm 0.3$ . Note that this value tightly satisfies the estimated lower bounds which were established by different procedures, namely by studying the IPR, the level spacing and the entanglement entropy. Although neither the study of the breakdown of ETH provides precise answers, we consider it the most reliable approach of those used in this work.

## VI. CONCLUSIONS

We introduced and studied a model which simulates a disordered system of interacting particles with spin  $1/2$ . The Hilbert space is isomorphic to the set of vertices of a hypercube. The Hamiltonian of this system is the sum of two parts. The first part is the adjacency matrix of a random graph, which is a subset of the edges of a hypercube and simultaneously it is a random regular graph with degree three, i.e. a random cubic graph. The second part is diagonal with independent Gaussian random numbers with tunable variance. Therefore, it

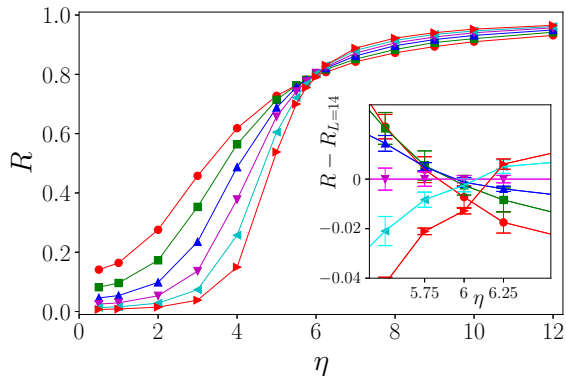


FIG. 19. Level-to-level fluctuations of the  $z$ -component of the local spin operator, as a function of the disorder strength. The levels were taken in a narrow interval around the center of the band  $\epsilon = 0$ . The system size is  $L = 8$  ( $\bullet$ ),  $10$  ( $\blacksquare$ ),  $12$  ( $\blacktriangle$ ),  $14$  ( $\blacktriangledown$ ),  $16$  ( $\blacktriangleleft$ ),  $18$  ( $\blacktriangleright$ ). In the inset, we show the detail of the area where the curves cross. For better visibility, we subtracted the data for  $L = 14$ .

can be seen as a special kind of a random-graph analog of the Rosenzweig-Porter random matrix ensemble. The comparison with the Rosenzweig-Porter (RP) ensemble must be taken with great care, though. First, our model corresponds rather to log-normal RP [129] than the classical RP ensemble. Second, having most matrix elements strictly zero, as is our case, could make a big difference from having random non-negative numbers, as is the case of log-normal RP. And third, the transition in RP ensembles is governed rather by the exponent in the scaling of matrix elements with size [128], while here the governing parameter is the amplitude of diagonal elements. This makes our model closer to the original work of Rosenzweig and Porter [127] than to the more recent investigations [128, 131]. Further comparison to RP ensembles would require deeper study which was not our aim here.

The random graph in question is created starting from a manifestly cubic graph by a sequence of random rewiring moves that preserve the degree of all affected vertices. This algorithm surely does not cover uniformly the whole set of random cubic graphs embedded in hypercube, but we believe it samples the set representatively enough. We tested that on a small system of dimension  $L = 5$  and we found no deviation from uniformly sampled set.

The properties of the model were investigated by exact diagonalization of many instances of the random Hamiltonian, for system sizes  $L \leq 18$ . The main question was the presence and properties of the localization transition. In this work we view the localization transition from a purely static perspective as an eigenstate transition, i.e. sudden qualitative change in the nature of the eigenvectors, when the strength of the disorder increases. This is reflected first in the inverse participation ratio (IPR). This way we found the estimated phase diagram in the plane energy-disorder and observed the mobility edge,

which separates the localized and delocalized regions. The disorder strength at which localization appears is highest at the center of the energy spectrum, thus marking the critical disorder  $\eta_c$ , beyond which all eigenvectors are localized. From the study of IPR, we obtained the lower bound  $\eta_c > 6$ . Close to the supposed transition we found clear sign of multifractality in eigenvectors. At the same time we consider the seemingly extended interval of disorder strengths which support multifractality in delocalized phase to be merely a finite-size effect and we expect this interval shrinks when size is further increased. However, much better numerical data would be necessary to see it with certainty.

We also used the classical signature of the change in the character of eigenvectors as reflected in the organization of energy levels. Indeed, the side-effect of localization is lifting the level repulsion which results in Poisson level-spacing distribution rather than the Wigner-like which is universal characteristic of delocalized phase. We observed the transition with all the well-known drawbacks, namely the marked shift of the predicted transition point to larger values when the system size increases. From this point of view our model behaves identically to both the random regular graphs and true interacting-particle models, like the disordered Heisenberg chain.

So, to this point our model reproduces what is known from the study of random regular graphs. The main point of our work, however, lies in extensions which are not accessible in random regular graphs with no extra properties. Specifically, our graphs allow, first, definition of entanglement entropy, and, second, study of the violation of eigenvalue thermalization hypothesis. The study of these two properties is the core of our contribution. Let us discuss them now.

The change in the nature of eigenvectors is visible in the entanglement entropy and entanglement spectrum. This appears when we look at a subsystem of the whole system, typically at an exact half. As the random graph we use is embedded in a  $L$ -dimensional hypercube, it is straightforward how to define the density matrix of the subsystem whose Hilbert space has dimension  $L/2$ . Note that this would be hardly possible for a generic random regular graph. We stress here the advantage of our approach. The entanglement entropy shows clear volume scaling with increasing  $L$  when in the delocalized phase, while the localized phase is characterized by surface scaling. Analyzing the flow diagram for increasing  $L$  in the delocalized phase we get a weaker lower bound for critical disorder,  $\eta_c > 5$ . In the localized phase, we observed the divergence of the asymptotic value of entanglement entropy in the form  $(\eta - \eta_c)^{-1}$  i.e. with the critical exponent  $\nu = 1$ . The critical disorder estimated this way was  $\eta_c = 5.6 \pm 0.2$ , which is slightly lower than the lower bound obtained from IPR. The possible explanation might be that the divergence is actually weaker, governed by lower exponent  $\nu < 1$ .

We are able to see not only the asymptotic behavior for  $L \rightarrow \infty$ , but also the leading finite size corrections which

are exponential in  $L$  and proportional to  $2^{-L/2}$  in both the localized and delocalized phases. The factors of proportionality are expected to diverge when we approach the critical point from either of the two sides. We indeed observed that the factors increase in both phases when coming closer to the transition, but without clear sign of the expected divergence. Larger systems would be necessary to see that effect, but with current algorithms there is little hope that we could go significantly beyond the maximum used here, which was  $L = 18$ . Thus, we found that the behavior of finite size corrections is a good sign of the existence of two distinct phases, the localized and the delocalized one, but it is not an efficient way to establish the transition point. Similarly, we found that the form of the entanglement spectrum clearly distinguishes between delocalized and localized phase. The delocalized phase is characterized by the Marčenko-Pastur exponent  $-1/2$  up to the cutoff which scales with the system size as  $O(2^{-L/2})$ . In the localized phase it is not possible to specify a single exponent, but rather the locally defined exponent of the entanglement spectrum decreases continuously from  $-1/2$  to about  $-1.2$  when the eigenvalues increase over several decades up to the maximum value, which is of order  $O(2^{-1})$  independently of system size. Unfortunately, the entanglement spectrum does not provide a quantitative tool for extracting the critical disorder value.

In this respect, we found that the much more efficient way is the study of the violation of the Eigenstate thermalization hypothesis (ETH). We found that the delocalized and localized phases are characterized by substantially different distribution of diagonal, as well as off-diagonal elements of local spin operators. We found that both diagonal and off-diagonal elements are normally distributed in the delocalized phase, in agreement with ETH. Moreover, the width of the Gaussian shrinks with increasing system size. On the contrary, in delocalized phase the distribution of diagonal elements is bimodal and the off-diagonal elements follow a power-law distribution. Therefore, we observe clear qualitative signs of the breakdown of ETH in the localized phase. Quantitatively, it is observed in the level-to-level fluctuations of the diagonal elements. This quantity is negligible in the delocalized phase but close to one in the delocalized phase. Indeed, high level-to-level fluctuations imply failure of ETH and lack of thermalization. Therefore, the quantity of these fluctuations may serve as order parameter for the localization transition. Contrary to the level-spacing statistics, here we do not observe significant shift of the crossing value with increasing size. Therefore, we consider the level-to-level fluctuations the best signature of localizations of those studied in this work. On this basis, we estimate the critical disorder as  $\eta_c = 6.1 \pm 0.3$ . This value is tightly above the lower bounds established from the study of IPR, so we consider these findings consistent.

One of the main motivations for this work came from the field of Many-body localization (MBL). Summariz-

ing our results, we conclude that we observed many of the characteristic features of MBL in our model, despite the fact that the random Hamiltonian of our spin model does not follow from an explicit particle-particle interaction, but rather it is taken from a very specific random matrix ensemble. This could imply that MBL is a generic phenomenon in certain class of random Hamiltonians. One of the keywords in the study of MBL is locality, or, equivalently, partitioning to subsystems. Indeed, ETH is formulated as a property of local operators, or operators whose support is limited to a small subsystem of the whole. Analogically, the entanglement entropy (EE) belongs to specific subsystems. The fact, that this subsystem is usually taken as exact half of the whole is mainly due to computational convenience and at the same time to practical impossibility to work with really big systems. Indeed, in abstract considerations the subsystem whose EE we calculate should be much smaller than the whole system, but still macroscopic. In practice, though, this is impossible to satisfy with systems as small as  $L \leq 18$ . However, the requirement of locality or partitioning imposes only quite general limits on the random matrix ensemble in question. The Hilbert space must be a tensor product of certain number of parts, each belonging to one possible partition, or to a support of one of the local operators. The Hamiltonian, then, is random, but must conform with this tensor product. The model we presented and studied in this work, is one simple example of such type of random Hamiltonians. Certainly more elaborate and even more general models may follow. We can for example think of two random graphs, corresponding to partitions  $A$  and  $B$ , and define a new graph simply taking tensor product of these two graphs, with possible cutting of certain percentage of links, in order to keep the average degree properly scaled. Studying entanglement entropy in such system would be in principle straightforward. Or, having system  $A$  much smaller, perhaps corresponding to one particle, or spin, only, this scheme would enable to study ETH with local operators acting only on the single particle in  $A$ .

This idea leads to the system of two parallel random regular graphs diagonally coupled to each other. As the random regular graphs are accessible to analytic means, like the replica trick, there is a hope that also such double random regular graph might be solvable. So, the model studied by us here can provide a starting point for deeper analysis. We show in the Appendix basic steps in the analytical study which may follow. We leave the investigation of such host of questions to future research.

## ACKNOWLEDGMENTS

Computational resources were provided by the e-INFRA CZ project (ID:90254), supported by the Ministry of Education, Youth and Sports of the Czech Republic.

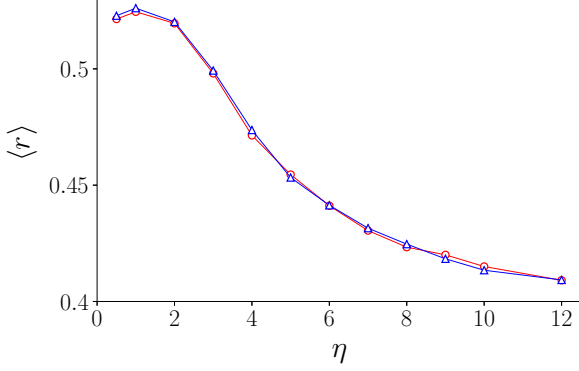


FIG. 20. Dependence of the averaged spacing ratio on the disorder strength, for dimension  $L = 5$ . The symbols  $\circ$  correspond to graphs created by rewiring algorithm, the symbols  $\triangle$  to graphs sampled uniformly.

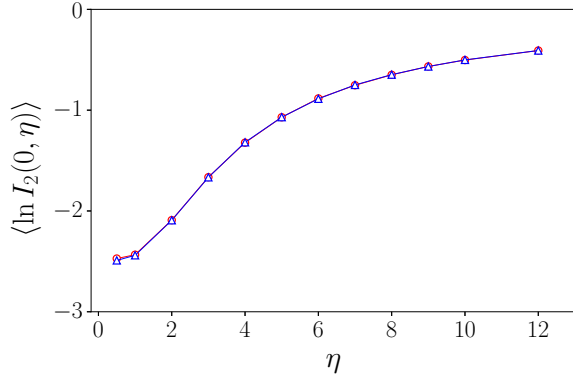


FIG. 21. Dependence of the inverse participation ratio at the center of the spectrum on the disorder strength, for dimension  $L = 5$ . The symbols  $\circ$  correspond to graphs created by rewiring algorithm, the symbols  $\triangle$  to graphs sampled uniformly.

#### Appendix A: Comparison of algorithms for graph creation

The number  $H_3(L)$  of cubic graphs embedded into hypercube grows very fast with dimension  $L$ . A very naive guess estimates this number as  $\sim L^{2^L}$ . Without loss of generality we can fix that the first vertex is connected to three vertices belonging to first three of  $L$  possible directions. The counts of possibilities mentioned later are given with such constraint. Trivially  $H_3(3) = 1$  and it is not difficult to find all such graphs for  $L = 4$ . We find  $H_3(4) = 68$ . All but one of these graphs are connected. Going one step further in dimension is already computationally intensive task. For  $L = 5$  we were able to enumerate all  $H_3(5) = 290701974$  cubic graphs embedded in five-dimensional hypercube and we found that only very small fraction of them are disconnected. The number of connected graphs was  $H_3^c(5) = 290475585$ . Proceeding to

$L = 6$  proved unfeasible (unless a significantly smarter algorithm is available).

The graphs created by random rewiring algorithm described in the main text do not sample the whole set of  $H_3^c(5)$  graphs, but we performed at least a partial check whether the rewiring-created graphs are representative enough. To this end, we took the whole set of  $H_3^c(5)$  graphs we explicitly found, and we selected from it samples randomly. This way we get uniformly-sampled set of graphs. We compare its properties to rewiring-created set of graphs with  $L = 5$  by adding random normally-distributed diagonal disorder to both sets and calculating two basic properties of the spectrum, namely the spacing distribution parameter  $\langle r \rangle$  and the IPR in the middle of the band (i.e. close to the eigenvalue 0). We show in Figs. 20 and 21 how these quantities depend on the disorder strength. We can see that the results for the uniformly-sampled set and for the rewiring-created set are nearly indistinguishable one from the other. We consider that a strong indication that the rewiring algorithm does not introduce any artifacts which would impact on the results of our work.

#### Appendix B: Perspective of analytic calculations in dimer graph

Any graph embedded in a hypercube of dimension  $L+1$  has natural dimer structure. Indeed, its vertex set is a union of vertex sets of two hypercubes of dimension  $L$ , while its edge set is the union of three components. The first two components are the subsets of edges of the first and second  $L$ -dimensional hypercube, and the third component is the subset of “diagonal” edges, which are those edges that connect mutually homomorphic vertices in the first and the second hypercube. This allows natural definition of the  $z$ -component of spin operator as diagonal matrix with  $+1$  on all vertices of the first hypercube and  $-1$  on all vertices of the second hypercube.

We can generalize this idea to wider classes of graphs, beyond the hypercube. Imagine two graphs homomorphic to each other in statistical sense. Obviously, the two graphs must have the same number of vertices. One example, which brings us back to the main subject of this paper are hypercubes with equal dimension and edges present or absent with the same probabilistic manner in both. Another, more amorphous example are two Erdős-Rényi graphs with the same edge probability. Then, we can make a dimer from this pair of graphs by joining the two by edges which are chosen from the set of “diagonal” edges. The existence of the homomorphism ensures the existence of such set. Typically, if there is a homomorphism, there are more of them. So, there is a multitude of ways to construct the dimer from two homomorphic graphs. In any of these cases, it is possible to define the  $z$ -component of spin operator as explained above. This opens the road to studying eigenvector thermalization hypothesis in random Hamiltonians based on such dimer

graphs.

The appeal of such approach is in its potential analytic solvability. We have no ambition to solve these problems in this paper, as our main focus was only on a numerical study of a single specific example of graphs which naturally have such dimer structure. However, we provide here at least a sketch of possible pathways in further simplified situations, where the Hamiltonian stemming from random graphs is replaced by random matrix and the randomly placed zeros and ones corresponding to “diagonal” edges are replaced by a constant number  $d$ , which reflects the relative occurrence of ones. Moreover, we limit ourselves only on extreme cases of fully localized and fully delocalized cases. The fully localized case is straightforward and provides an information on size dependence, while the fully delocalized case needs the use of replica trick and provides just infinite-size result.

### 1. Fully localized case

Let us denote the two components of the dimer  $A$  and  $B$ . Suppose that each of the components has  $N$  vertices. The capital indexes  $I, J, \dots \in \{A, B\}$  will denote components, lowercase indices  $i, j, \dots \in \{1, 2, \dots, N\}$  will denote vertices within the components. In fully localized phase the Hamiltonian can be approximated as

$$H_{iIjJ} = \eta \delta_{IJ} \delta_{ij} \xi_{Ii} + d(1 - \delta_{IJ}) \delta_{ij} \quad (\text{B1})$$

where  $\xi_{Ii}$  are independent Gaussian random variables with unit variance. The parameter  $\eta$  quantifies the strength of the disorder. In the same basis, the  $z$ -component of the spin operator is the matrix

$$\sigma_{zIiJj} = \delta_{IJ} \delta_{ij} (-1)^I \quad (\text{B2})$$

with convention  $(-1)^A = 1$ ,  $(-1)^B = -1$ .

Diagonalization of the Hamiltonian is trivial, as it splits into  $N$  uncoupled  $2 \times 2$  matrices. Equally trivial is the calculation of the average of the spin  $\langle \sigma_z \rangle_\lambda$  in an eigenstate with eigenvalue  $\lambda$ . The probability of this average with respect of the Gaussian disorder  $\xi_{Ii}$  and over all eigenvectors is then

$$P(\langle \sigma_z \rangle) = \frac{d}{\sqrt{\pi} \eta} \frac{\exp\left(-\left(\frac{d}{\eta}\right)^2 \frac{\langle \sigma_z \rangle^2}{1 - \langle \sigma_z \rangle^2}\right)}{(1 - \langle \sigma_z \rangle^2)^{3/2}}. \quad (\text{B3})$$

The mean of  $\langle \sigma_z \rangle$  is of course zero due to symmetry. The second moment can be computed in terms of the series in powers of  $(d/\eta)^2$ , namely

$$\overline{\langle \sigma_z \rangle^2} = 1 - \frac{1}{2} \left(\frac{d}{\eta}\right)^2 + \frac{3}{16} \left(\frac{d}{\eta}\right)^4 - \dots \quad (\text{B4})$$

The dependence on the system size enters through the parameter  $d$ , which measures the fraction of edges among all potential diagonal links. In random cubic graph in a hypercube we have  $N = 2^L$ , each vertex has  $L$  potential

links within its own component and one diagonal link. The diagonal link has therefore (for large  $L$ ) probability  $\simeq 3/(L+1)$  to be occupied by edge. This suggests the scaling  $d \propto 1/\ln N$ . This should be compared with the behavior of the numerically established quantity  $R$  defined in (26). On the basis of (B4) we expect that

$$1 - R \sim \frac{1}{L^2 \eta^2} \quad (\text{B5})$$

for large  $L$  and deep in the localized phase.

### 2. Sketch of the replica calculations in fully delocalized case

In contrast to the localized case, in the fully delocalized phase the Hamiltonian can be approximated by a composition from two GOE random matrices, connected diagonally as in the localized case. Therefore, we take

$$H_{iIjJ} = \eta \delta_{IJ} A_{ij}^{(I)} + d(1 - \delta_{IJ}) \delta_{ij} \quad (\text{B6})$$

where  $A^{(I)}$  are  $N \times N$  GOE random matrices with unit variance, i.e.

$$P(A_{ij}^{(I)}) = \sqrt{\frac{N}{2g\pi}} e^{-\frac{1}{2g} N (A_{ij}^{(I)})^2} \quad (\text{B7})$$

and  $g = 1$  for  $i \neq j$ ,  $g = 2$  for  $i = j$ .

We can proceed in a standard manner, applying the replica method. (From the numerous literature, let us mention e.g. [131, 138] and references therein.) The first step is the calculation of the resolvent  $R(\zeta) = (\zeta - H)^{-1}$ ,  $\zeta \in \mathbb{C}$ , which is directly related to the averaged density of eigenvalues

$$\overline{\mathcal{D}}(E) = \frac{1}{\pi} \lim_{\epsilon \rightarrow 0^+} \text{Im} \overline{\text{Tr} R(E - i\epsilon)} \quad (\text{B8})$$

(here and in the following the bar denotes average over disorder). We can similarly calculate the quantity

$$\overline{\mathcal{D}_z}(E) = \frac{1}{\pi} \lim_{\epsilon \rightarrow 0^+} \text{Im} \overline{\text{Tr} \sigma_z R(E - i\epsilon)} \quad (\text{B9})$$

and from it deduce the average of the  $z$ -component of the spin operator at energy  $E$

$$\overline{\langle \sigma_z \rangle}_E = \frac{\overline{\mathcal{D}_z}(E)}{\overline{\mathcal{D}}(E)}. \quad (\text{B10})$$

Note the seemingly inconsistent replacement of average of a fraction by fraction of averages. In fact, for however large but finite  $N$  this is the only sensible way to compute  $\overline{\langle \sigma_z \rangle}_E$ , because before averaging neither  $\mathcal{D}_z(E)$  nor  $\mathcal{D}(E)$  are continuous functions of  $E$  but just collections of  $\delta$ -functions.

Anyway, we expect that  $\overline{\langle \sigma_z \rangle}_E = 0$ , unless there is a mechanism for breaking the symmetry between components  $A$  and  $B$  of the dimer. We assume it is excluded here, and the same would hold even if localization occurs. Therefore, the quantity of interest is a more complicated object, which is the second moment  $\overline{\langle \sigma_z \rangle}_E^2$ . It can be computed applying the same trick as used in calculation of the inverse participation ratio [119, 139]. The core quantity is the disorder-averaged product of resolvents taken at two complex-conjugated points. If  $R(\zeta_+)R(\zeta_-)$  is known, we can compute  $\mathcal{R}^{(2)}(\zeta_+, \zeta_-) =$

$\sum_{IJij} (-1)^{I+J} \overline{R_{IiIi}(\zeta_+) R_{JjJj}(\zeta_-)}$  and from here

$$\overline{\langle \sigma_z \rangle}_E^2 = \lim_{\epsilon \rightarrow 0^+} \frac{\epsilon \mathcal{R}^{(2)}(E + i\epsilon, E - i\epsilon)}{\text{Im} \overline{\text{Tr} R(E - i\epsilon)}} \quad (\text{B11})$$

The key point in proving this formula consists, as shown in [139], in the fact that the double sum over eigenvalues, which is present in the product  $R(\zeta_+)R(\zeta_-)$ , in fact reduces to a single sum, because only terms with both eigenvalues equal survive the limit  $\epsilon \rightarrow 0$ .

The quantities  $\overline{\text{Tr} R(\zeta)}$  and  $\mathcal{R}^{(2)}(\zeta_+, \zeta_-)$  are calculated using the replica trick. As a first step we define the replicated partition functions

$$Z(\zeta; n) = \int e^{-\frac{1}{2} \zeta \sum_{Ii} \sum_{a=1}^n (\phi_{Ii}^a)^2} \exp \left( \frac{1}{2} \sum_{IJ} \sum_{a=1}^n \phi_{Ii}^a H_{IJ} \phi_{Jj}^a \right) d[\phi_{Ii}^a] \quad (\text{B12})$$

$$Z^{(2)}(\zeta_+, \zeta_-, \tilde{\zeta}_+, \tilde{\zeta}_-; n) = \int e^{-\frac{1}{2} \sum_{s=\pm} \sum_{Ii} (\zeta_s + (-1)^I \tilde{\zeta}_s) \sum_{a=1}^n (\phi_{Iis}^a)^2} \exp \left( \frac{1}{2} \sum_{s=\pm} \sum_{IJ} \sum_{a=1}^n \phi_{Iis}^a H_{IJ} \phi_{Jjs}^a \right) d[\phi_{Iis}^a] \quad (\text{B13})$$

Here we use the abbreviations  $d[\phi_{Ii}^a] = \prod_{Ii} \prod_{a=1}^n d\phi_{Ii}^a$ ,  $d[\phi_{Iis}^a] = \prod_{Ii} \prod_{s=\pm} \prod_{a=1}^n d\phi_{Iis}^a$ . The density of states is then

$$\overline{\mathcal{D}}(E) = \frac{2}{\pi} \lim_{\epsilon \rightarrow 0^+} \text{Im} \left( \frac{\partial}{\partial \zeta} \lim_{n \rightarrow 0} \frac{\partial}{\partial n} Z(\zeta; n) \right)_{\zeta=E+i\epsilon} \quad (\text{B14})$$

and the averaged double resolvent

$$\mathcal{R}^{(2)}(\zeta_+, \zeta_-) = 4 \lim_{\zeta_{\pm} \rightarrow 0} \frac{\partial^2}{\partial \zeta_+ \partial \zeta_-} \lim_{n \rightarrow 0} \frac{\partial}{\partial n} Z^{(2)}. \quad (\text{B15})$$

(We omitted the arguments of  $Z^{(2)}$  to lighten the notation.) Further procedure is standard [138]. Let us first show how it works for the density of states. In the  $N \rightarrow \infty$  limit we apply the saddle point method, which leads to minimization of the free energy

$$\mathcal{F} = \frac{1}{2} \sum_I \sum_{ab} (q_{ab}^I)^2 + \frac{1}{2} \ln \det M \quad (\text{B16})$$

with respect to the two  $n \times n$  matrices with elements  $q_{ab}^I$ . Here  $M$  is square matrix  $(2n) \times (2n)$  with elements

$$M_{IaJb} = (\zeta \delta_{ab} - \sqrt{2} \eta q_{ab}^I) \delta_{IJ} - d \delta_{ab} (1 - \delta_{IJ}). \quad (\text{B17})$$

Assuming replica symmetry  $q_{ab}^I = \bar{q}^I \delta_{ab} - \bar{q}^I$  we obtain at the end

$$\overline{\mathcal{D}}(E) = \frac{2}{\pi \eta} \lim_{\epsilon \rightarrow 0^+} \text{Im} Q(E - i\epsilon) \quad (\text{B18})$$

where  $Q(\zeta)$  is the solution of the cubic equation

$$Q = \frac{\frac{\zeta}{\eta} - Q}{\left(\frac{\zeta}{\eta} - Q\right)^2 - \left(\frac{d}{\eta}\right)^2}. \quad (\text{B19})$$

In the course of the calculations it turns out that the off-diagonal elements are all zero,  $\tilde{q}^I = 0$ . The same procedure can be used in calculation of  $\overline{\mathcal{D}}_z(E)$ . The result is explicitly zero, as expected.

Similar procedure is used in calculation of  $Z^{(2)}$  and then  $\mathcal{R}^{(2)}$ . Formally, it is nearly equal, with free energy

$$\mathcal{F} = \frac{1}{2} \sum_{Iss'} \sum_{ab} (q_{ab}^{Iss'})^2 + \frac{1}{2} \ln \det M \quad (\text{B20})$$

and  $(4n) \times (4n)$  matrix

$$M_{IsaJs'b} = ((\zeta_s + (-1)^I \tilde{\zeta}_s) \delta_{ss'} \delta_{ab} - \sqrt{2} \eta q_{ab}^{Iss'}) \delta_{IJ} - d \delta_{ss'} \delta_{ab} (1 - \delta_{IJ}). \quad (\text{B21})$$

Technically, however, it is more complicated, because we have to minimize the free energy with respect to eight  $n \times n$  matrices  $q^{Iss'}$ . Even using the symmetry  $s \leftrightarrow s'$  and assuming replica-symmetric solution, leads to minimization with respect to six variables  $\bar{q}^{I++}, \bar{q}^{I+-}, \bar{q}^{I--}$ , where  $I = A, B$ . (As in the calculation of the density of states, the off-diagonal elements of the replica-symmetric matrices turn out to be zero explicitly). Let us show the key steps of the replica-symmetric calculation. We can define the  $4 \times 4$  matrix  $m$  with elements

$$m_{IJs's'} = ((\zeta_s + (-1)^I \tilde{\zeta}_s) \delta_{ss'} - \sqrt{2} \eta \bar{q}^{Iss'}) \delta_{IJ} - d \delta_{ss'} (1 - \delta_{IJ}). \quad (\text{B22})$$

We also define the auxiliary constant matrices with

$$T^{Iss'} = -\frac{1}{\sqrt{2} \eta} \frac{\partial m}{\partial \bar{q}^{Iss'}} \quad (\text{B23})$$

and

$$V^s = \frac{\partial m}{\partial \tilde{\zeta}_s}. \quad (\text{B24})$$

All matrix elements of these matrices are either 0 or 1 or  $-1$  and they are useful for making the formulas compact. Then, the set of equations for the parameters of the replica-symmetric solution is

$$\bar{q}^{Iss'} = \frac{\eta}{\sqrt{2}} \text{Tr} m^{-1} T^{Iss'}. \quad (\text{B25})$$

This is a set of six independent algebraic equations of

fifth order. When solved, we can insert them to find  $Z^{(2)}$  and by derivation with respect to  $\tilde{\zeta}_+$  and  $\tilde{\zeta}_-$  we obtain the formula for  $\mathcal{R}^{(2)}$ . To this end, we first need the  $8 \times 8$  matrix  $G$ , whose inverse is found explicitly

$$(G^{-1})_{Is_1s_2 Js'_1s'_2} = \delta_{IJ} \delta_{s_1s'_1} \delta_{s_2s'_2} + \eta^2 \text{Tr} T^{Is_1s_2} m^{-1} T^{Js'_1s'_2} m^{-1}. \quad (\text{B26})$$

Finally, we obtain

$$\begin{aligned} \mathcal{R}^{(2)}(\zeta_+, \zeta_-) = & 2 \text{Tr} V^+ m^{-1} V^- m^{-1} - \\ & - 2\eta^2 \sum_{Is_1s_2} \sum_{Js'_1s'_2} \left( \text{Tr} V^+ m^{-1} T^{Is_1s_2} m^{-1} \right) G_{Is_1s_2 Js'_1s'_2} \left( \text{Tr} V^- m^{-1} T^{Js'_1s'_2} m^{-1} \right) \end{aligned} \quad (\text{B27})$$

where we assumed that the limit  $\tilde{\zeta}_\pm \rightarrow 0$  was taken, so the right-hand side is function of  $\zeta_+$  and  $\zeta_-$  only.

The formulas listed above solve the problem of computing the second moment of the  $z$ -component of local spin. However, it has non-zero value only on condition that  $\mathcal{R}^{(2)}(E + i\epsilon, E - i\epsilon)$  diverges for  $\epsilon \rightarrow 0$ . In the calculation of inverse participation ratio this happens in the localized phase. In our case, there is no source of such divergence. Therefore, after performing the limit  $\epsilon \rightarrow 0$  in (B11) we get  $\langle \sigma_z \rangle_E^2 = 0$ . In fact, this is exactly what was expected in the delocalized phase. However, this holds only in the  $N \rightarrow \infty$  limit and it would be highly desirable to compute finite size effects, in order to compare it to the simulation results. This is a considerably more involved project. The first and most obvious source of finite-size corrections is the fluctuation around the minimum of  $\mathcal{F}$ . This can be obtained by calculating the Hessian matrix at the replica-symmetric minimum and then performing the Gaussian integration. However, there is also another possible source of finite-size effects. Indeed, as showed in [138], in a typical situation there are also replica-symmetry-broken solutions with contribution of the order  $1/N$ . And even worse, there is whole manifold

of such solutions and it is indispensable to integrate over entire such manifold. We expect that the experience from [138] will apply also in our case. We have no ambition of making such calculations in this work, so we stop at this stage.

Let us finish with a perspective to possible future calculations. Here we used a dimer of coupled GOE matrices. It is natural to extend the random-matrix ensemble further in order to allow for localized states. One such choice is the Rosenzweig-Porter ensemble, which was (besides the supersymmetric approach, see e.g. [128]) recently solved also by replica method [131]. So, we propose to make a dimer of two Rosenzweig-Porter matrices and observe the localization transition in the behavior of  $\langle \sigma_z \rangle_E^2$ , as sketched in the calculations above. However, one important observation is due here. In many earlier works on Rosenzweig-Porter matrices the transition is driven by the exponent determining the scaling of matrix elements with system size  $N$ . On the contrary, in our case the transition is driven by noise strength  $\eta$ . In fact, this is just how the problem was formulated in the founding paper of Rosenzweig and Porter [127]. It is the latter formulation that is relevant for our purposes.

- 
- [1] L. D. Landau and E. M. Lifshitz, *Statistical Physics*, *Statistical Physics* (Butterworth-Heinemann, Oxford, 1980).
  - [2] S. S. Kondov, W. R. McGehee, W. Xu, and B. DeMarco, Disorder-Induced Localization in a Strongly Correlated Atomic Hubbard Gas, *Phys. Rev. Lett.* **114**, 083002 (2015).
  - [3] M. Schreiber, S. S. Hodgman, P. Bordia, H. P. Lüschen, M. H. Fischer, R. Vosk, E. Altman, U. Schneider, and I. Bloch, Observation of many-body localization of inter-

- acting fermions in a quasirandom optical lattice, *Science* **349**, 842 (2015).
- [4] G. A. Álvarez, D. Suter, and R. Kaiser, Localization-delocalization transition in the dynamics of dipolar-coupled nuclear spins, *Science* **349**, 846 (2015).
- [5] A. M. Kaufman, M. E. Tai, A. Lukin, M. Rispoli, R. Schittko, P. M. Preiss, and M. Greiner, Quantum thermalization through entanglement in an isolated many-body system, *Science* **353**, 794 (2016).
- [6] J.-Y. Choi, S. Hild, J. Zeiher, P. Schauß, A. Rubio-

- Abadal, T. Yefsah, V. Khemani, D. A. Huse, I. Bloch, and C. Gross, Exploring the many-body localization transition in two dimensions, *Science* **352**, 1547 (2016).
- [7] P. Bordia, H. P. Lüschen, S. S. Hodgman, M. Schreiber, I. Bloch, and U. Schneider, Coupling Identical one-dimensional Many-Body Localized Systems, *Phys. Rev. Lett.* **116**, 140401 (2016).
- [8] J. Smith, A. Lee, P. Richerme, B. Neyenhuis, P. W. Hess, P. Hauke, M. Heyl, D. A. Huse, and C. Monroe, Many-body localization in a quantum simulator with programmable random disorder, *Nature Physics* **12**, 907 (2016).
- [9] H. P. Lüschen, P. Bordia, S. Scherg, F. Alet, E. Altman, U. Schneider, and I. Bloch, Observation of Slow Dynamics near the Many-Body Localization Transition in One-Dimensional Quasiperiodic Systems, *Phys. Rev. Lett.* **119**, 260401 (2017).
- [10] P. Bordia, H. Lüschen, S. Scherg, S. Gopalakrishnan, M. Knap, U. Schneider, and I. Bloch, Probing Slow Relaxation and Many-Body Localization in Two-Dimensional Quasiperiodic Systems, *Phys. Rev. X* **7**, 041047 (2017).
- [11] P. Bordia, H. Lüschen, U. Schneider, M. Knap, and I. Bloch, Periodically driving a many-body localized quantum system, *Nature Physics* **13**, 460 (2017).
- [12] K. X. Wei, C. Ramanathan, and P. Cappellaro, Exploring Localization in Nuclear Spin Chains, *Phys. Rev. Lett.* **120**, 070501 (2018).
- [13] K. Xu, J.-J. Chen, Y. Zeng, Y.-R. Zhang, C. Song, W. Liu, Q. Guo, P. Zhang, D. Xu, H. Deng, K. Huang, H. Wang, X. Zhu, D. Zheng, and H. Fan, Emulating Many-Body Localization with a Superconducting Quantum Processor, *Phys. Rev. Lett.* **120**, 050507 (2018).
- [14] A. Rubio-Abadal, J.-Y. Choi, J. Zeiher, S. Hollerith, J. Rui, I. Bloch, and C. Gross, Many-Body Delocalization in the Presence of a Quantum Bath, *Phys. Rev. X* **9**, 041014 (2019).
- [15] T. Kohlert, S. Scherg, X. Li, H. P. Lüschen, S. Das Sarma, I. Bloch, and M. Aidelsburger, Observation of Many-Body Localization in a One-Dimensional System with a Single-Particle Mobility Edge, *Phys. Rev. Lett.* **122**, 170403 (2019).
- [16] M. Rispoli, A. Lukin, R. Schittko, S. Kim, M. E. Tai, J. Léonard, and M. Greiner, Quantum critical behaviour at the many-body localization transition, *Nature* **573**, 385 (2019).
- [17] A. Lukin, M. Rispoli, R. Schittko, M. E. Tai, A. M. Kaufman, S. Choi, V. Khemani, J. Léonard, and M. Greiner, Probing entanglement in a many-body-localized system, *Science* **364**, 256 (2019).
- [18] T. Brydges, A. Elben, P. Jurcevic, B. Vermersch, C. Maier, B. P. Lanyon, P. Zoller, R. Blatt, C. F. Roos, Probing Rényi entanglement entropy via randomized measurements, *Science* **364**, 260 (2019).
- [19] Q. Guo, C. Cheng, Z.-H. Sun, Z. Song, H. Li, Z. Wang, W. Ren, H. Dong, D. Zheng, Y.-R. Zhang, R. Mondaini, H. Fan, and H. Wang, Observation of energy-resolved many-body localization, *Nature Physics* **17**, 234 (2021).
- [20] M. Gong, G. D. de Moraes Neto, C. Zha, Y. Wu, H. Rong, Y. Ye, S. Li, Q. Zhu, S. Wang, Y. Zhao, F. Liang, J. Lin, Y. Xu, C.-Z. Peng, H. Deng, A. Bayat, X. Zhu, and J.-W. Pan, Experimental characterization of the quantum many-body localization transition, *Phys. Rev. Research* **3**, 033043 (2021).
- [21] J. L. C. da C. Filho, Z. Gonzalez Izquierdo, A. Saguia, T. Albash, I. Hen, and M. S. Sarandy, Localization transition induced by programmable disorder, *Phys. Rev. B* **105**, 134201 (2022).
- [22] S. Aubry and G. André, Analyticity breaking and Anderson localization in incommensurate lattices, *Annals of the Israel Physical Society* **3**, 133 (1980).
- [23] R. Islam, R. Ma, P. M. Preiss, M. E. Tai, A. Lukin, M. Rispoli, and M. Greiner, Measuring entanglement entropy in a quantum many-body system, *Nature* **528**, 77 (2015).
- [24] P. W. Anderson, Absence of diffusion in certain random lattices, *Phys. Rev.* **109**, 1492 (1958).
- [25] H. Kunz and B. Souillard, The localization transition on the Bethe lattice, *J. Physique Letters* **44**, L-411 (1983).
- [26] I. V. Gornyi, A. D. Mirlin, and D. G. Polyakov, Interacting Electrons in Disordered Wires: Anderson Localization and Low-T Transport, *Phys. Rev. Lett.* **95**, 206603 (2005).
- [27] D. M. Basko, I. L. Aleiner, and B. L. Altshuler, Metal-insulator transition in a weakly interacting many-electron system with localized single-particle states, *Ann. Phys.* **321**, 1126 (2006).
- [28] R. Abou-Chacra, P. W. Anderson, and D. J. Thouless, A selfconsistent theory of localization, *J. Phys. C: Solid State Phys.* **6**, 1734 (1973).
- [29] V. Oganesyan and D. A. Huse, Localization of interacting fermions at high temperature, *Phys. Rev. B* **75**, 155111 (2007).
- [30] M. Žnidarič, T. Prosen, and P. Prelovšek, Many-body localization in the Heisenberg XXZ magnet in a random field, *Phys. Rev. B* **77**, 064426 (2008).
- [31] A. Pal and D. A. Huse, Many-body localization phase transition, *Phys. Rev. B* **82**, 174411 (2010).
- [32] C. Monthus and T. Garel, Many-body localization transition in a lattice model of interacting fermions: Statistics of renormalized hoppings in configuration space, *Phys. Rev. B* **81**, 134202 (2010).
- [33] T. C. Berkelbach and D. R. Reichman, Conductivity of disordered quantum lattice models at infinite temperature: Many-body localization, *Phys. Rev. B* **81**, 224429 (2010).
- [34] J. H. Bardarson, F. Pollmann, and Joel E. Moore., Unbounded Growth of Entanglement in Models of Many-Body Localization, *Phys. Rev. Lett.* **109**, 017202 (2012).
- [35] M. Serbyn, Z. Papić, and D. A. Abanin, Universal Slow Growth of Entanglement in Interacting Strongly Disordered Systems, *Phys. Rev. Lett.* **110**, 260601 (2013).
- [36] A. De Luca and A. Scardicchio, Ergodicity breaking in a model showing many-body localization, *EPL* **101**, 37003 (2013).
- [37] S. Iyer, V. Oganesyan, G. Refael, and D. A. Huse, Many-body localization in a quasiperiodic system, *Phys. Rev. B* **87**, 134202 (2013).
- [38] R. Vosk and E. Altman, Many-Body Localization in One Dimension as a Dynamical Renormalization Group Fixed Point, *Phys. Rev. Lett.* **110**, 067204 (2013).
- [39] J. A. Kjäll, J. H. Bardarson, and F. Pollmann, Many-Body Localization in a Disordered Quantum Ising Chain, *Phys. Rev. Lett.* **113**, 107204 (2014).
- [40] M. Serbyn, Z. Papić, and D. A. Abanin, Quantum quenches in the many-body localized phase, *Phys. Rev. B* **90**, 174302 (2014).
- [41] Arun Nanduri, Hyungwon Kim, and David A. Huse, Entanglement spreading in a many-body localized system,

- Phys. Rev. B **90**, 064201 (2014).
- [42] F. Andraschko, T. Enss, and J. Sirker, Purification and Many-Body Localization in Cold Atomic Gases, *Phys. Rev. Lett.* **113**, 217201 (2014).
  - [43] P. Ponte, Z. Papić, F. Huveneers, and D. A. Abanin, Many-Body Localization in Periodically Driven Systems, *Phys. Rev. Lett.* **114**, 140401 (2015).
  - [44] R. Modak and S. Mukerjee, Many-Body Localization in the Presence of a Single-Particle Mobility Edge, *Phys. Rev. Lett.* **115**, 230401 (2015).
  - [45] Y. Bar Lev, G. Cohen, and D. R. Reichman, Absence of Diffusion in an Interacting System of Spinless Fermions on a One-Dimensional Disordered Lattice, *Phys. Rev. Lett.* **114**, 100601 (2015).
  - [46] D. J. Luitz, N. Laflorencie, and F. Alet, Many-body localization edge in the random-field Heisenberg chain, *Phys. Rev. B* **91**, 081103(R) (2015).
  - [47] E. Baygan, S. P. Lim, and D. N. Sheng, Many-body localization and mobility edge in a disordered spin-1/2 Heisenberg ladder, *Phys. Rev. B* **92**, 195153 (2015).
  - [48] I. Mondragon-Shem, A. Pal, T. L. Hughes, and C. R. Laumann, Many-body mobility edge due to symmetry-constrained dynamics and strong interactions, *Phys. Rev. B* **92**, 064203 (2015).
  - [49] X. Li, S. Ganeshan, J. H. Pixley, and S. Das Sarma, Many-Body Localization and Quantum Nonergodicity in a Model with a Single-Particle Mobility Edge, *Phys. Rev. Lett.* **115**, 186601 (2015).
  - [50] M. Serbyn, Z. Papić, and D. A. Abanin, Criterion for Many-Body Localization-Delocalization Phase Transition, *Phys. Rev. X* **5**, 041047 (2015).
  - [51] K. Agarwal, S. Gopalakrishnan, M. Knap, M. Müller, and E. Demler, Anomalous Diffusion and Griffiths Effects Near the Many-Body Localization Transition, *Phys. Rev. Lett.* **114**, 160401 (2015).
  - [52] E. J. Torres-Herrera and L. F. Santos, Dynamics at the many-body localization transition, *Phys. Rev. B* **92**, 014208 (2015).
  - [53] M. Friesdorf, A. H. Werner, W. Brown, V. B. Scholz, and J. Eisert, Many-Body Localization Implies that Eigenvectors are Matrix-Product States, *Phys. Rev. Lett.* **114**, 170505 (2015).
  - [54] T. Orell, A. A. Michailidis, M. Serbyn, and M. Silveri, Probing the many-body localization phase transition with superconducting circuits, *Phys. Rev. B* **100**, 134504 (2019).
  - [55] X. Wei, C. Cheng, G. Xianlong, and R. Mondaini, Investigating many-body mobility edges in isolated quantum systems, *Phys. Rev. B* **99**, 165137 (2019).
  - [56] N. Macé, F. Alet, and N. Laflorencie, Multifractal Scalings Across the Many-Body Localization Transition, *Phys. Rev. Lett.* **123**, 180601 (2019).
  - [57] M. Hopjan, G. Orso, and F. Heidrich-Meisner, Detecting delocalization-localization transitions from full density distributions, *Phys. Rev. B* **104**, 235112 (2021).
  - [58] Y. Bar Lev, D. R. Reichman, and Y. Sagi, Many-body localization in system with a completely delocalized single-particle spectrum, *Phys. Rev. B* **94**, 201116(R) (2016).
  - [59] P. Sierant, D. Delande, and J. Zakrzewski, Many-body localization due to random interactions, *Phys. Rev. A* **95**, 021601(R) (2017).
  - [60] N. Macé, N. Laflorencie and F. Alet, Many-body localization in a quasiperiodic Fibonacci chain, *SciPost Phys.* **6**, 050 (2019).
  - [61] M. Brenes, M. Dalmonte, M. Heyl, and A. Scardicchio, Many-Body Localization Dynamics from Gauge Invariance, *Phys. Rev. Lett.* **120**, 030601 (2018).
  - [62] J. Z. Imbrie, On Many-Body Localization for Quantum Spin Chains, *J. Stat. Phys.* **163**, 998 (2016).
  - [63] V. Ros, M. Müller, and A. Scardicchio, Integrals of motion in the many-body localized phase, *Nuclear Physics B* **891**, 420 (2015).
  - [64] R. Sims and G. Stolz, Many-Body Localization: Concepts and Simple Models, *Markov Processes and Related Fields* **21**, 791 (2015).
  - [65] G. Stolz, Aspects of the mathematical theory of disordered quantum spin chains, *Analytic Trends in Mathematical Physics* **741**, 163 (2020).
  - [66] V. Chulaevsky and Y. Suhov, Multi-particle Anderson Localisation: Induction on the Number of Particles, *Math. Phys. Anal. Geom.* **12**, 117 (2009).
  - [67] T. Ekanga, Localization in multiparticle Anderson models with weak interaction, *Theoretical and Mathematical Physics* **206**, 357 (2021).
  - [68] D. A. Huse, R. Nandkishore, and V. Oganesyan, Phenomenology of fully many-body-localized systems, *Phys. Rev. B* **90**, 174202 (2014).
  - [69] M. Serbyn, Z. Papić, and D. A. Abanin, Local Conservation Laws and the Structure of the Many-Body Localized States, *Phys. Rev. Lett.* **111**, 127201 (2013).
  - [70] A. Chandran, I. H. Kim, G. Vidal, and D. A. Abanin, Constructing local integrals of motion in the many-body localized phase, *Phys. Rev. B* **91**, 085425 (2015).
  - [71] L. Rademaker and M. Ortuño, Explicit Local Integrals of Motion for the Many-Body Localized State, *Phys. Rev. Lett.* **116**, 010404 (2016).
  - [72] T. E. O'Brien, D. A. Abanin, G. Vidal, and Z. Papić, Explicit construction of local conserved operators in disordered many-body systems, *Phys. Rev. B* **94**, 144208 (2016).
  - [73] J. Z. Imbrie, V. Ros, and A. Scardicchio, Local integrals of motion in many-body localized systems, *Ann. Phys. (Berlin)* **529**, 1600278 (2017).
  - [74] L. Rademaker, M. Ortuño, and A. M. Somoza, Many-body localization from the perspective of Integrals of Motion, *Ann. Phys. (Berlin)* **529**, 1600322 (2017).
  - [75] S. Gopalakrishnan and R. Nandkishore, Mean-field theory of nearly many-body localized metals, *Phys. Rev. B* **90**, 224203 (2014).
  - [76] R. Nandkishore, S. Gopalakrishnan, and D. A. Huse, Spectral features of a many-body-localized system weakly coupled to a bath, *Phys. Rev. B* **90**, 064203 (2014).
  - [77] D. J. Luitz, F. Huveneers, and W. De Roeck, How a Small Quantum Bath Can Thermalize Long Localized Chains, *Phys. Rev. Lett.* **119**, 150602 (2017).
  - [78] A. C. Potter, R. Vasseur, and S. A. Parameswaran, Universal Properties of Many-Body Delocalization Transitions, *Phys. Rev. X* **5**, 031033 (2015).
  - [79] R. Vosk, D. A. Huse, and E. Altman, Theory of the Many-Body Localization Transition in One-Dimensional Systems, *Phys. Rev. X* **5**, 031032 (2015).
  - [80] S. Gopalakrishnan, M. Müller, V. Khemani, M. Knap, E. Demler, and D. A. Huse, Low-frequency conductivity in many-body localized systems, *Phys. Rev. B* **92**, 104202 (2015).
  - [81] S. Gopalakrishnan, K. Agarwal, E. A. Demler, D. A.

- Huse, and M. Knap, Griffiths effects and slow dynamics in nearly many-body localized systems, *Phys. Rev. B* **93**, 134206 (2016).
- [82] W. De Roeck and F. Huveneers, Stability and instability towards delocalization in many-body localization systems, *Phys. Rev. B* **95**, 155129 (2017).
- [83] T. Thiery, F. Huveneers, M. Müller, and W. De Roeck, Many-Body Delocalization as a Quantum Avalanche, *Phys. Rev. Lett.* **121**, 140601 (2018).
- [84] Alan Morningstar, Luis Colmenarez, Vedika Khemani, David J. Luitz, and David A. Huse, Avalanches and many-body resonances in many-body localized systems, *Phys. Rev. B* **105**, 174205 (2022).
- [85] W. De Roeck, F. Huveneers, M. Müller, and M. Schiulaz, Absence of many-body mobility edges, *Phys. Rev. B* **93**, 014203 (2016).
- [86] B. Bauer and C. Nayak, Area laws in a many-body localized state and its implications for topological order, *J. Stat. Mech.*, P09005 (2013).
- [87] D. N. Page, Average entropy of a subsystem, *Phys. Rev. Lett.* **71**, 1291 (1993).
- [88] F. Pietracaprina, G. Parisi A. Mariano, S. Pascasio and A. Scardicchio, Entanglement critical length at the many-body localization transition, *J. Stat. Mech.*, 113102 (2017).
- [89] V. A. Marčenko and L. A. Pastur, Distribution of eigenvalues for some sets of random matrices, *Math. USSR-Sbornik* **1**, 457 (1967).
- [90] Z.-C. Yang, C. Chamon, A. Hamma, and E. R. Mucchio, Two-Component Structure in the Entanglement Spectrum of Highly Excited States, *Phys. Rev. Lett.* **115**, 267206 (2015).
- [91] M. Serbyn, A. A. Michailidis, D. A. Abanin, and Z. Papić, Power-Law Entanglement Spectrum in Many-Body Localized Phases, *Phys. Rev. Lett.* **117**, 160601 (2016).
- [92] S. D. Geraedts, R. Nandkishore, and N. Regnault, Many-body localization and thermalization: Insights from the entanglement spectrum, *Phys. Rev. B* **93**, 174202 (2016).
- [93] S. D. Geraedts, N. Regnault, and R. M. Nandkishore, Characterizing the many-body localization transition using the entanglement spectrum, *New J. Phys.* **19**, 113021 (2017).
- [94] W. Buijsman, V. Gritsev, and V. Cheianov, Gumbel statistics for entanglement spectra of many-body localized eigenstates, *Phys. Rev. B* **100**, 205110 (2019).
- [95] G. De Chiara, S. Montangero, P. Calabrese, and R. Fazio, Entanglement entropy dynamics of Heisenberg chains, *J. Stat. Mech.*, P03001 (2006).
- [96] J. M. Deutsch, Quantum statistical mechanics in a closed system, *Phys. Rev. A* **43**, 2046 (1991).
- [97] Mark Srednicki, Chaos and quantum thermalization, *Phys. Rev. E* **50**, 888 (1994).
- [98] M. Rigol, V. Dunjko, and M. Olshanii, Thermalization and its mechanism for generic isolated quantum systems, *Nature* **452**, 854 (2008).
- [99] P. Reimann, Eigenstate thermalization: Deutsch's approach and beyond, *New J. Phys.* **17**, 055025 (2015).
- [100] D. J. Luitz, Long tail distributions near the many-body localization transition, *Phys. Rev. B* **93**, 134201 (2016).
- [101] R. K. Panda, A. Scardicchio, M. Schulz, S. R. Taylor, and M. Žnidarič, Can we study the many-body localization transition?, *EPL* **128**, 67003 (2019).
- [102] M. Goihl, J. Eisert, and C. Krumnow, Exploration of the stability of many-body localized systems in the presence of a small bath, *Phys. Rev. B* **99**, 195145 (2019).
- [103] J. Šuntajs, J. Bonča, T. Prosen, and L. Vidmar, Quantum chaos challenges many-body localization, *Phys. Rev. E* **102**, 062144 (2020).
- [104] P. Sierant, . Delande, and J. Zakrzewski, Thouless Time Analysis of Anderson and Many-Body Localization Transitions, *Phys. Rev. Lett.* **124**, 186601 (2020).
- [105] P. Sierant and J. Zakrzewski, Challenges to observation of many-body localization, *Phys. Rev. B* **105**, 224203 (2022).
- [106] P. Sierant, M. Lewenstein, and J. Zakrzewski, Polynomially Filtered Exact Diagonalization Approach to Many-Body Localization, *Phys. Rev. Lett.* **125**, 156601 (2020).
- [107] R. Nandkishore and D. A. Huse, Many-Body Localization and Thermalization in Quantum Statistical Mechanics, *Annu. Rev. Cond. Matter Phys.* **6**, 15 (2015).
- [108] E. Altman and R. Vosk, Universal Dynamics and Renormalization in Many-Body-Localized Systems, *Annu. Rev. Condens. Matter Phys.* **6**, 383 (2015).
- [109] D. A. Abanin and Z. Papić, Recent progress in many-body localization, *Ann. Phys. (Berlin)* **529**, 1700169 (2017).
- [110] D. J. Luitz and Y. Bar Lev, The ergodic side of the many-body localization transition, *Ann. Phys. (Berlin)* **529**, 1600350 (2017).
- [111] K. Agarwal, E. Altman, E. Demler, S. Gopalakrishnan, D. A. Huse, and M. Knap, rare-region effects and dynamics near the many-body localization transition, *Ann. Phys. (Berlin)* **529**, 1600326 (2017).
- [112] E. Altman, Many-body localization and quantum thermalization, *Nature Physics* **14**, 979 (2018).
- [113] F. Alet and N. Laflorencie, Many-body localization: An introduction and selected topics, *Comptes Rendus Physique* **19**, 498 (2018).
- [114] D. A. Abanin, E. Altman, I. Bloch, and M. Serbyn, Many-body localization, thermalization, and entanglement, *Rev. Mod. Phys.* **91**, 021001 (2019).
- [115] S. Gopalakrishnan and S.A. Parameswaran, Dynamics and transport at the threshold of many-body localization, *Phys. Rep.* **862**, 1 (2020).
- [116] G. Biroli, G. Semerjian, and M. Tarzia, Anderson model on Bethe lattices: density of states, localization properties and isolated eigenvalue, *Prog. Theor. Phys. Suppl.* **184**, 187 (2010).
- [117] A. De Luca, B. L. Altshuler, V. E. Kravtsov, and A. Scardicchio, Anderson Localization on the Bethe Lattice: Nonergodicity of Extended States, *Phys. Rev. Lett.* **113**, 046806 (2014).
- [118] M. Sonner, K. S. Tikhonov, and A. D. Mirlin, Multifractality of wave functions on a Cayley tree: From root to leaves, *Phys. Rev. B* **96**, 214204 (2017).
- [119] F. Slanina, Localization of eigenvectors in random graphs, *Eur. Phys. J. B* **85**, 361 (2012).
- [120] B. L. Altshuler, E. Cuevas, L. B. Ioffe, and V. E. Kravtsov, Nonergodic Phases in Strongly Disordered Random Regular Graphs, *Phys. Rev. Lett.* **117**, 156601 (2016).
- [121] K. S. Tikhonov, A. D. Mirlin, and M. A. Skvortsov, Anderson localization on random regular graphs, *Phys. Rev. B* **94**, 220203 (2016).
- [122] Giuseppe De Tomasi, Soumya Bera, Antonello Scardic-

- chio, and Ivan M. Khaymovich, Subdiffusion in the Anderson model on the random regular graph, *Phys. Rev. B* **101**, 100201 (2020).
- [123] K. S. Tikhonov and A. D. Mirlin, Statistics of eigenstates near the localization transition on random regular graphs, *Phys. Rev. B* **99**, 024202 (2019).
- [124] K. S. Tikhonov and A. D. Mirlin, Critical behavior at the localization transition on random regular graphs, *Phys. Rev. B* **99**, 214202 (2019).
- [125] K. S. Tikhonov and A. D. Mirlin, Eigenstate correlations around the many-body localization transition, *Phys. Rev. B* **103**, 064204 (2021).
- [126] K. S. Tikhonov and A. D. Mirlin, From Anderson localization on random regular graphs to many-body localization, *Annals of Physics* **435**, 168525 (2021).
- [127] N. Rosenzweig and C. E. Porter, "Repulsion of Energy Levels" in Complex Atomic Spectra, *Phys. Rev.* **120**, 1698 (1960).
- [128] V. E. Kravtsov, I. M. Khaymovich, E. Cuevas and M. Amini, A random matrix model with localization and ergodic transitions, *New J. Phys.* **17**, 122002 (2015).
- [129] I. M. Khaymovich, V. E. Kravtsov, B. L. Altshuler, and L. B. Ioffe, Fragile extended phases in the log-normal Rosenzweig-Porter model, *Phys. Rev. Research* **2**, 043346 (2020).
- [130] G. Biroli and M. Tarzia, Lévy-Rosenzweig-Porter random matrix ensemble, *Phys. Rev. B* **103**, 104205 (2021).
- [131] D. Venturelli, L. F. Cugliandolo, G. Schehr, and M. Tarzia, Replica approach to the generalized Rosenzweig-Porter model, *SciPost Phys.* **14**, 110 (2023).
- [132] F. Monteiro, T. Micklitz, M. Tezuka, and A. Altland, Minimal model of many-body localization, *Phys. Rev. Research* **3**, 013023 (2021).
- [133] I. García-Mata, J. Martin, O. Giraud, B. Georgeot, R. Dubertrand, and G. Lemarié, Critical properties of the Anderson transition on random graphs: Two-parameter scaling theory, Kosterlitz-Thouless type flow, and many-body localization, *Phys. Rev. B* **106**, 214202 (2022).
- [134] A. Morningstar and D. A. Huse, Renormalization-group study of the many-body localization transition in one dimension, *Phys. Rev. B* **99**, 224205 (2019).
- [135] P. T. Dumitrescu, A. Goremykina, S. A. Parameswaran, M. Serbyn, and R. Vasseur, Kosterlitz-Thouless scaling at many-body localization phase transitions, *Phys. Rev. B* **99**, 094205 (2019).
- [136] A. Goremykina, R. Vasseur, and M. Serbyn, Analytically Solvable Renormalization Group for the Many-Body Localization Transition, *Phys. Rev. Lett.* **122**, 040601 (2019).
- [137] F. Slanina, Localization in random bipartite graphs: Numerical and empirical study, *Phys. Rev. E* **95**, 052149 (2017).
- [138] A. Kamenev and M. Mézard, Wigner-Dyson statistics from the replica method, *J. Phys. A: Math. Gen.* **32**, 4373 (1999).
- [139] F. L. Metz, I. Neri, and D. Bollé, Localization transition in symmetric random matrices, *Phys. Rev. E* **82**, 031135 (2010).